Synthesis of Unsupported d^1-d^x Oxido Bridged Heterobimetallic Complexes Containing V^{IV}: A New Direction for Metal-to-Metal Charge Transfer

Xinyuan Wu, Tao Huang, Travis T. Lekich, Roger D. Sommer, Walter W. Weare.*

Department of Chemistry, North Carolina State University, Campus Box 8204, Raleigh, NC, 27695-8204, USA.

Table of contents

Electronic Absorption Spectra with Molar Absorptivity

The molar absorptivity was measured in dichloromethane under the protection of nitrogen at room temperature. The ε of **2c** and **2e** were measured in acetonitrile because of the poor solubility in dichloromethane. The ε of **2d** could not be obtained due to the low solubility in all common solvents, therefore an EAS spectra of **2d** is reported as a normalized absorbance.

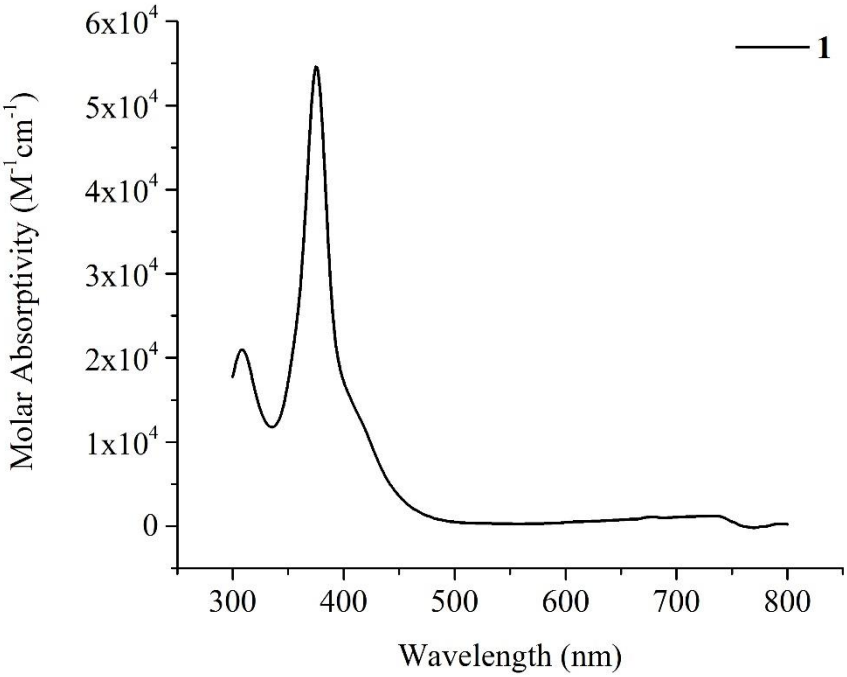

Figure S1. Electronic absorption spectrum of (TMTAA)V═O (**1**).

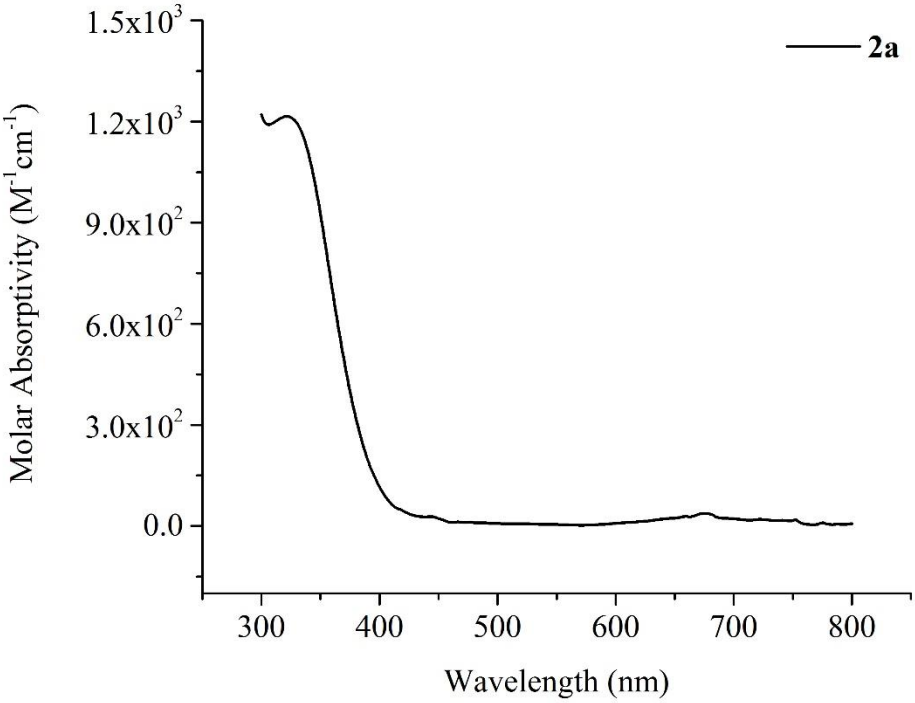

Figure S2. Electronic absorption spectrum of $[Mn(Py_5Me_2)](CF_3SO_3)_2$ (**2a**).

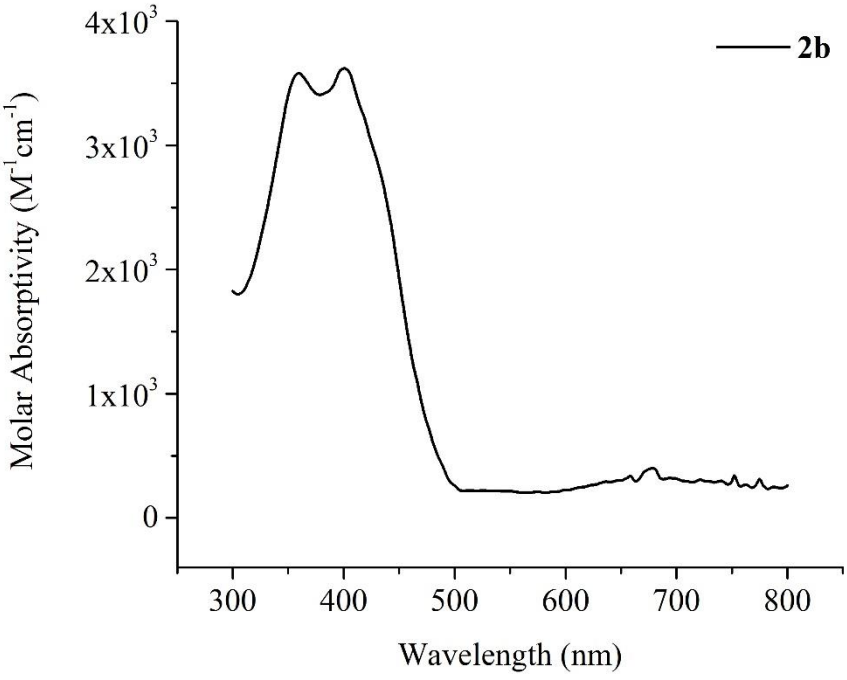

Figure S3. Electronic absorption spectrum of $[Fe(Py_5Me_2)](CF_3SO_3)_2$ (**2b**).

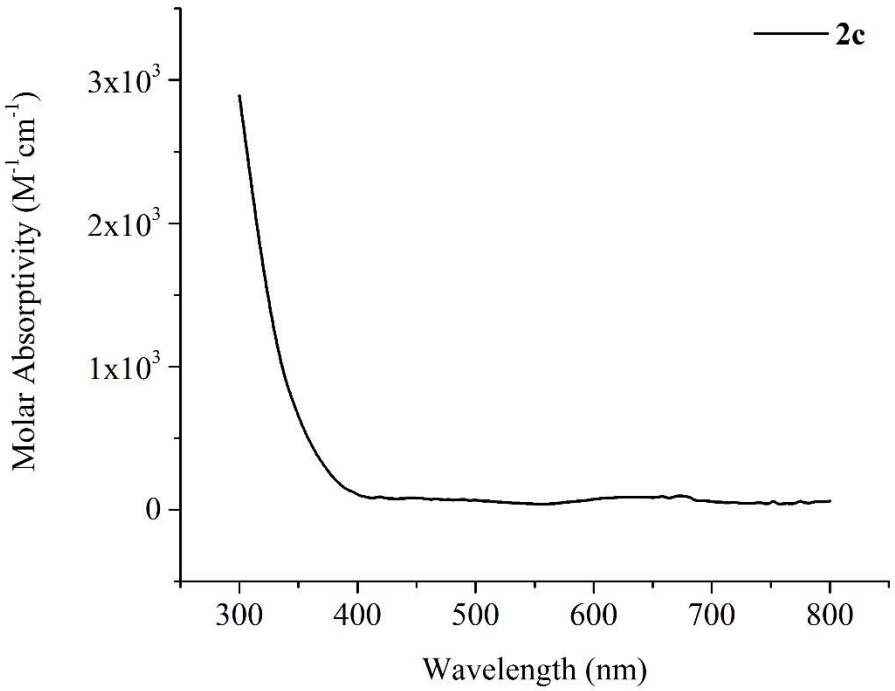

Figure S4. Electronic absorption spectrum of $[Co(H_2O)(Py_5Me_2)](CF_3SO_3)_2$ (**2c**).

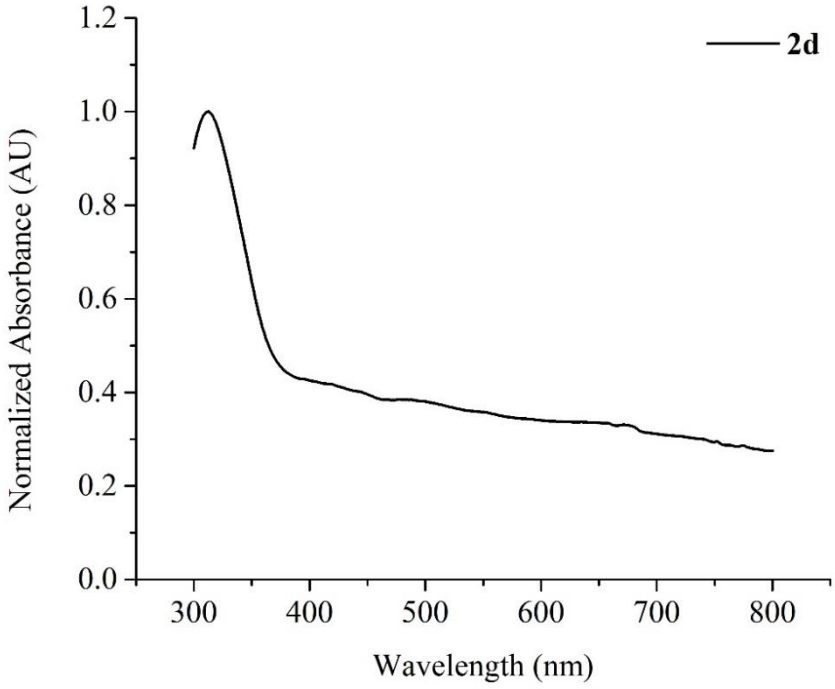

Figure S5. Electronic absorption spectrum of $[Ni(Py_5Me_2)](CF_3SO_3)_2$ (**2d**).

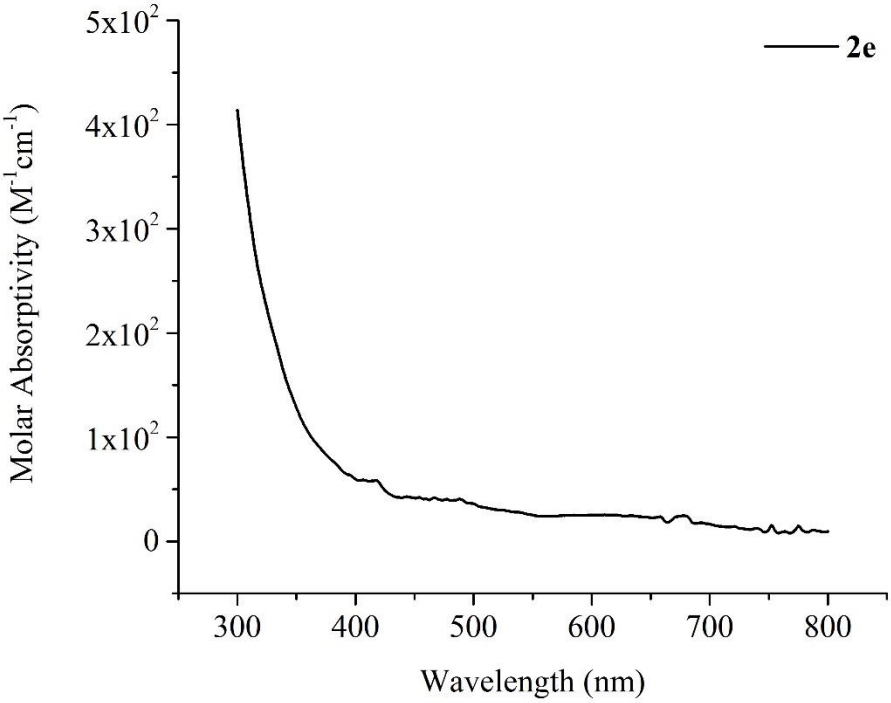

Figure S6. Electronic absorption spectrum of $[Cu(Py_5Me_2)](CF_3SO_3)_2$ (**2e**).

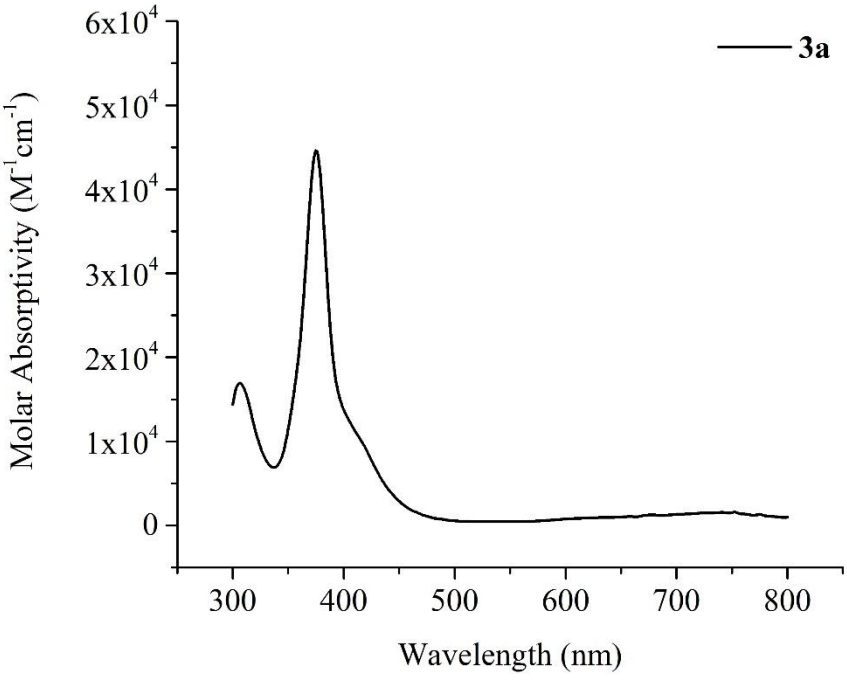

Figure S7. Electronic absorption spectrum of $[(TMTAA]V{=}O{\rightarrow}Mn(Py_5Me_2)](CF_3SO_3)_2$ (**3a**).

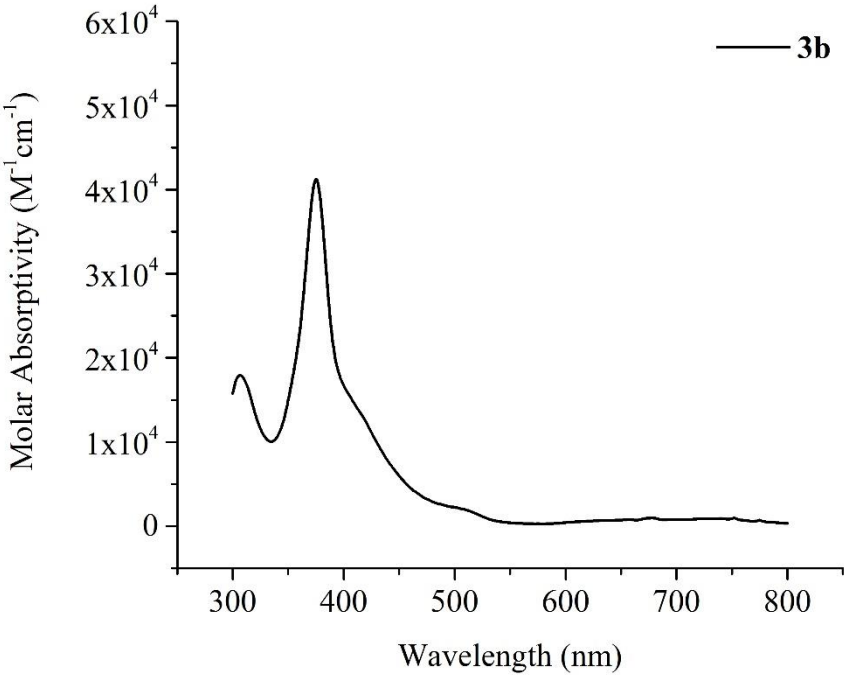

Figure S8. Electronic absorption spectrum of [(TMTAA]V═O→Fe(Py$_5$Me$_2$)](CF$_3$SO$_3$)$_2$ (**3b**).

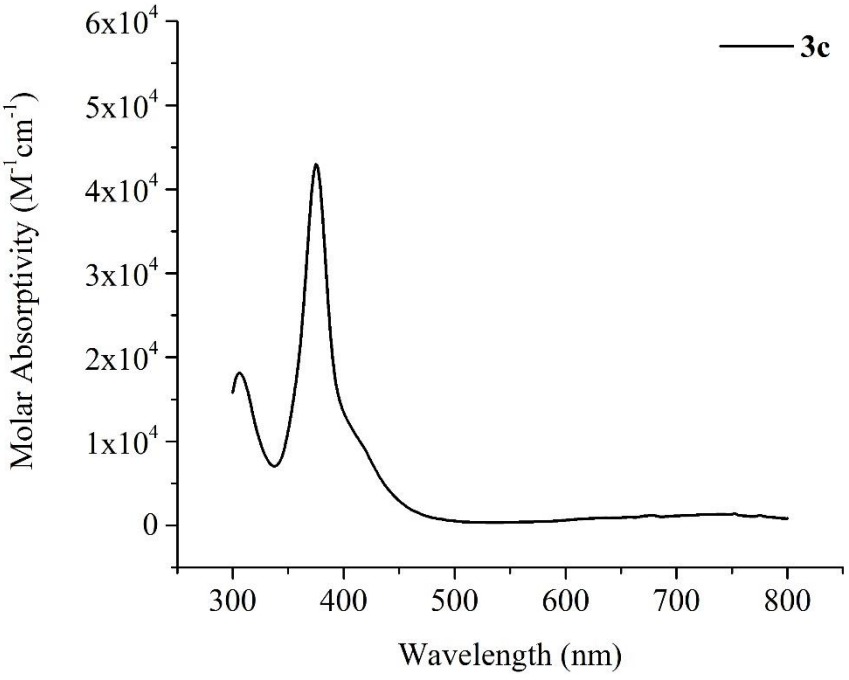

Figure S9. Electronic absorption spectrum of [(TMTAA]V═O→Co(Py$_5$Me$_2$)](CF$_3$SO$_3$)$_2$ (**3c**).

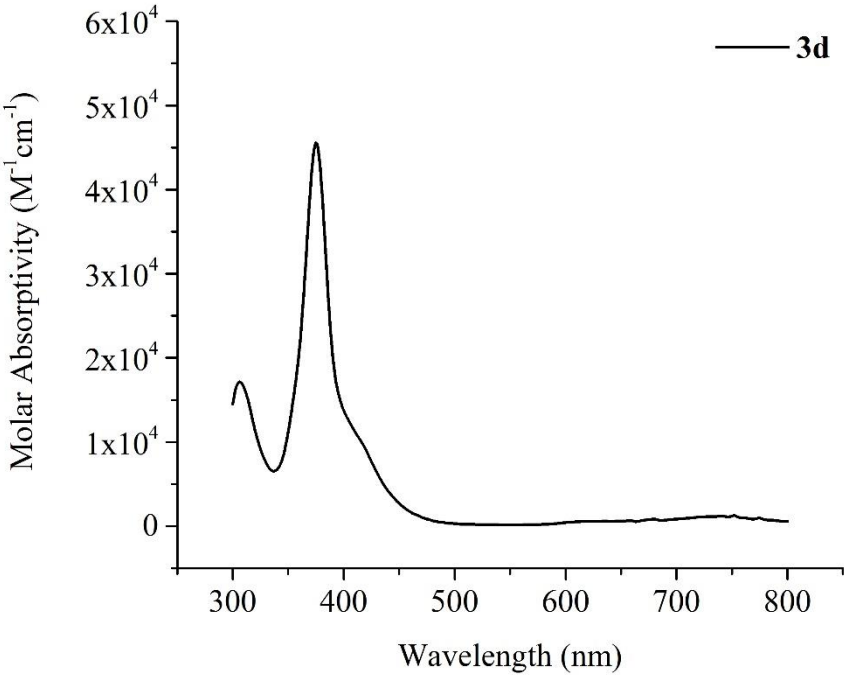

Figure S10. Electronic absorption spectrum of [(TMTAA]V═O→Ni(Py_5Me_2)](CF_3SO_3)$_2$ (**3d**).

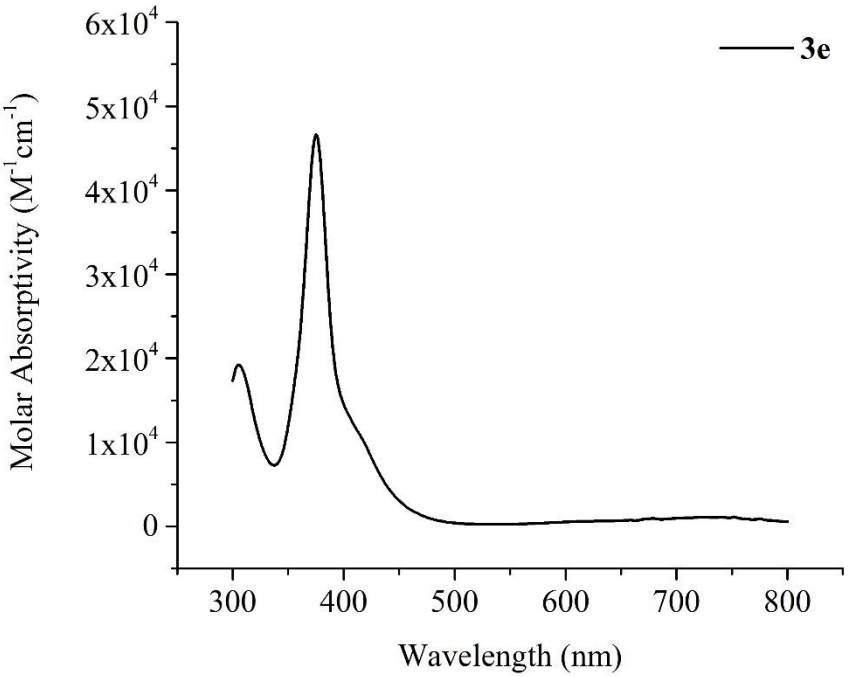

Figure S11. Electronic absorption spectrum of [(TMTAA]V═O→Cu(Py_5Me_2)](CF_3SO_3)$_2$ (**3e**).

Solid State ATR-FTIR Spectra

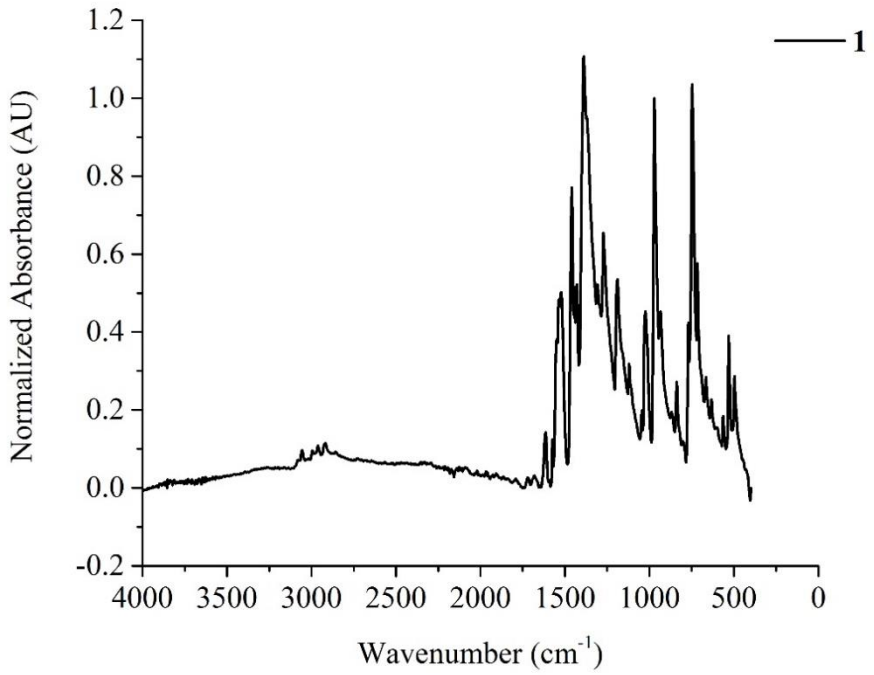

Figure S12. Solid State ATR-FTIR spectrum of (TMTAA)V═O (**1**).

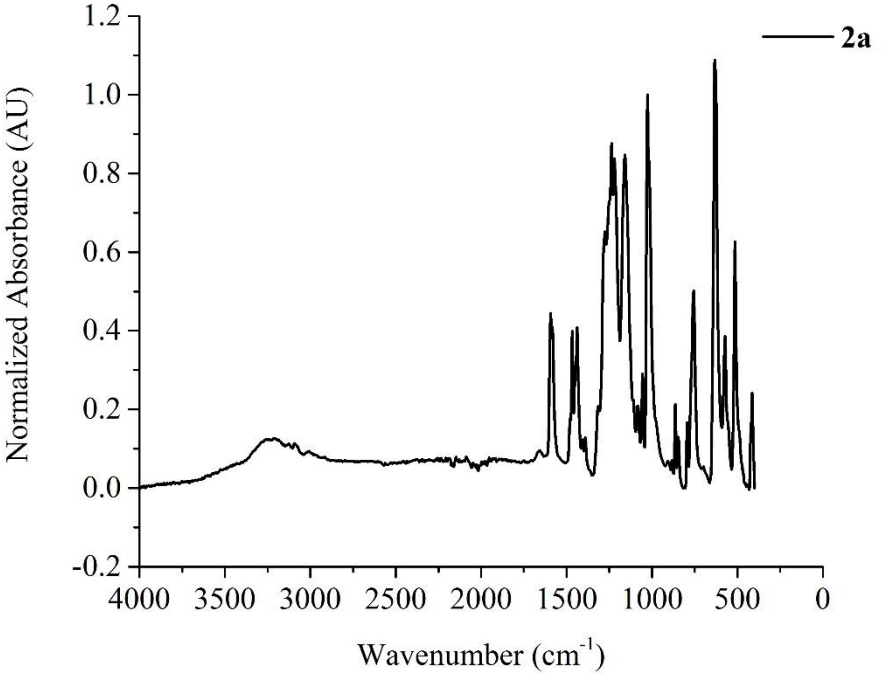

Figure S13. Solid State ATR-FTIR spectrum of $[Mn(Py_5Me_2)](CF_3SO_3)_2$ (**2a**).

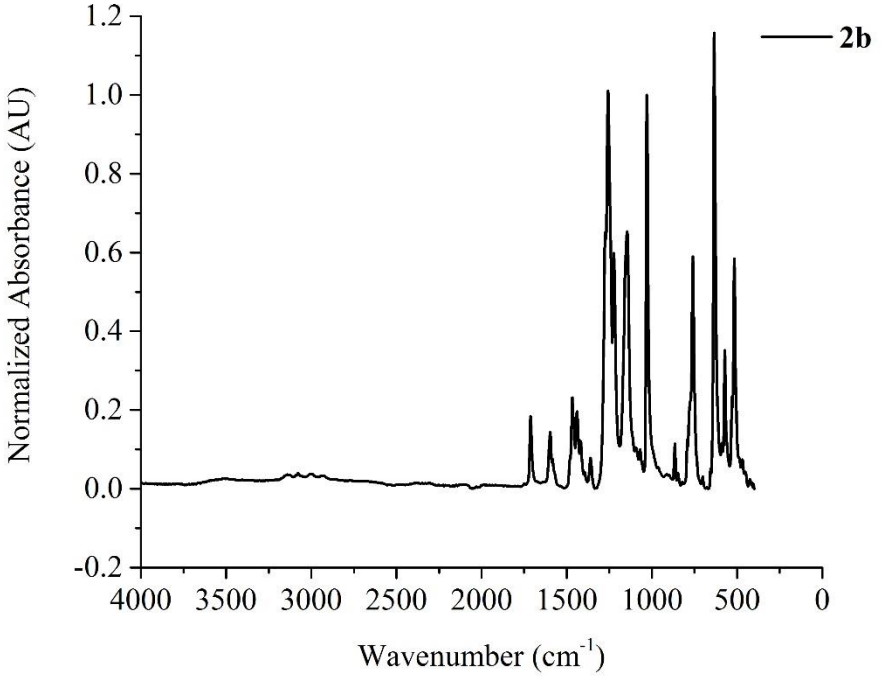

Figure S14. Solid State ATR-FTIR spectrum of $[Fe(Py_5Me_2)](CF_3SO_3)_2$ (**2b**).

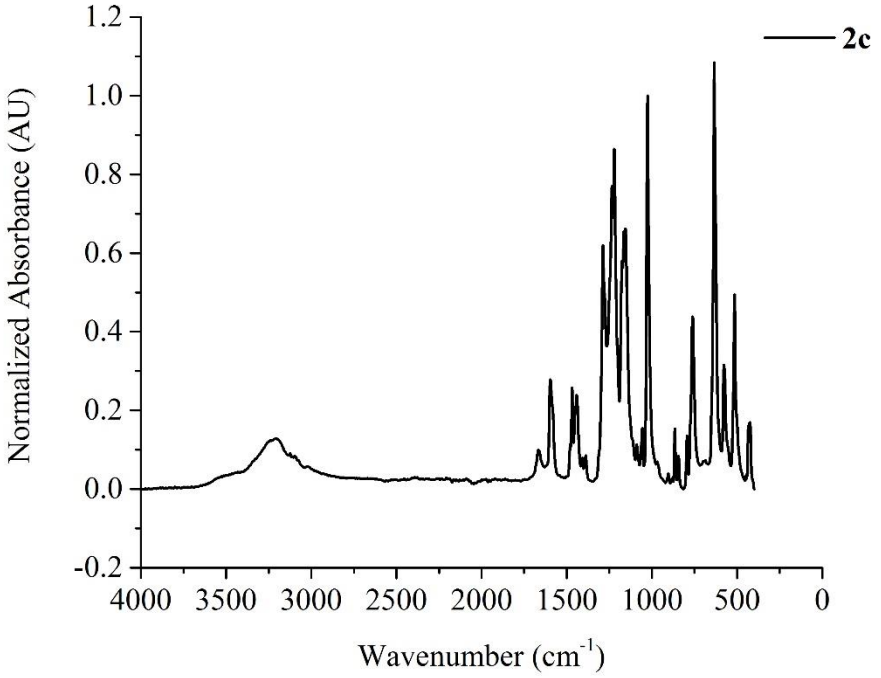

Figure S15. Solid State ATR-FTIR spectrum of $[Co(H_2O)(Py_5Me_2)](CF_3SO_3)_2$ (**2c**).

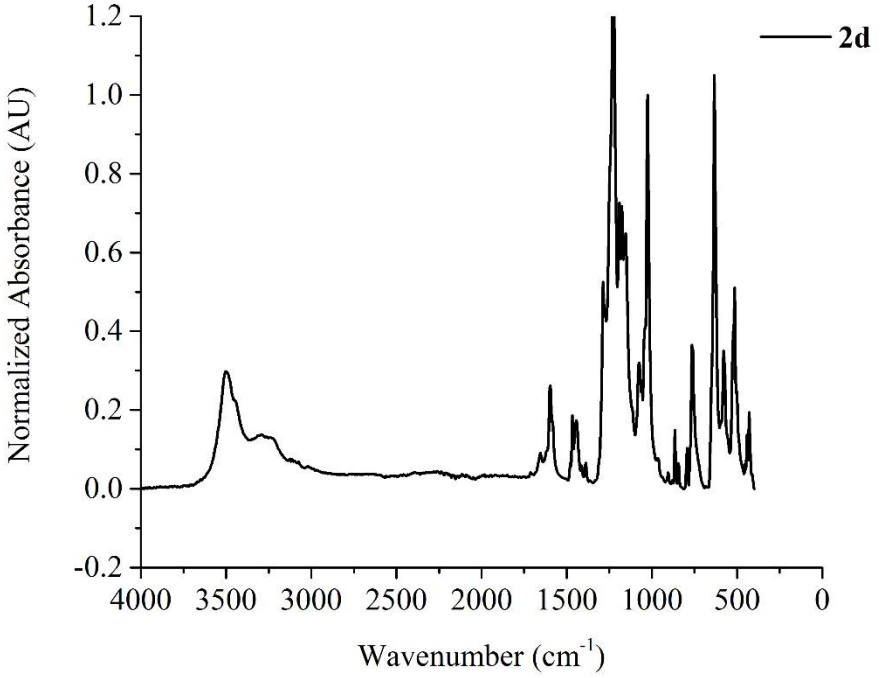

Figure S16. Solid State ATR-FTIR spectrum of $[Ni(Py_5Me_2)](CF_3SO_3)_2$ (**2d**).

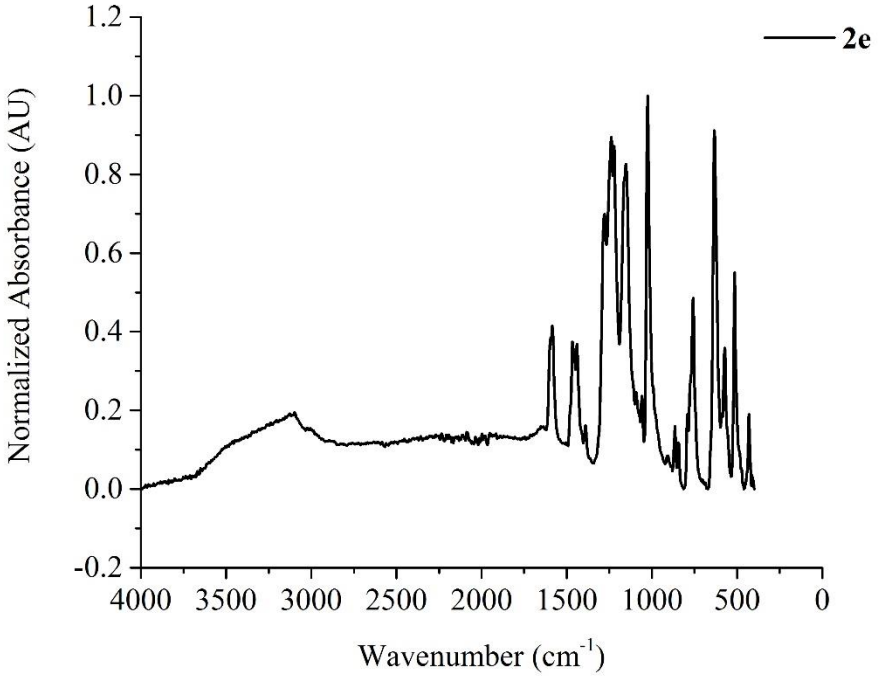

Figure S17. Solid State ATR-FTIR spectrum of $[Cu(Py_5Me_2)](CF_3SO_3)_2$ (**2e**).

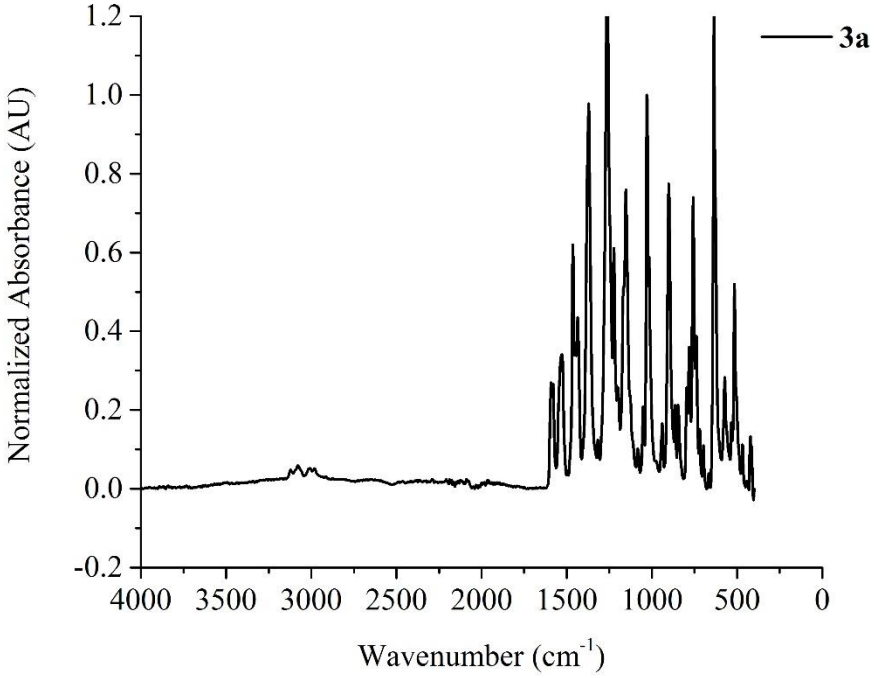

Figure S18. Solid State ATR-FTIR spectrum of [(TMTAA]V═O→Mn(Py_5Me_2)]($(CF_3SO_3)_2$ (**3a**).

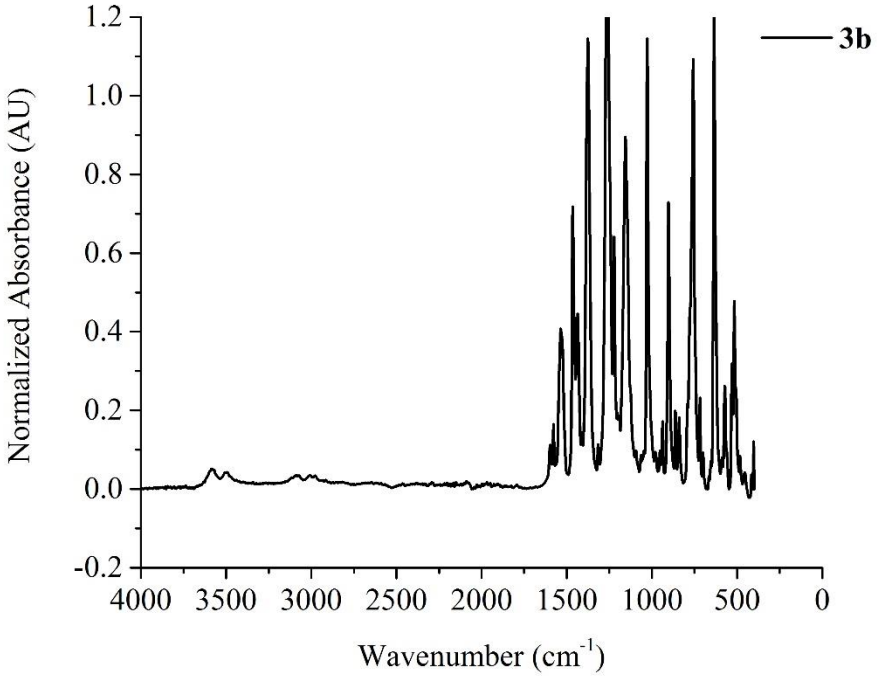

Figure S19. Solid State ATR-FTIR spectrum of [(TMTAA]V═O→Fe(Py_5Me_2)]($(CF_3SO_3)_2$ (**3b**).

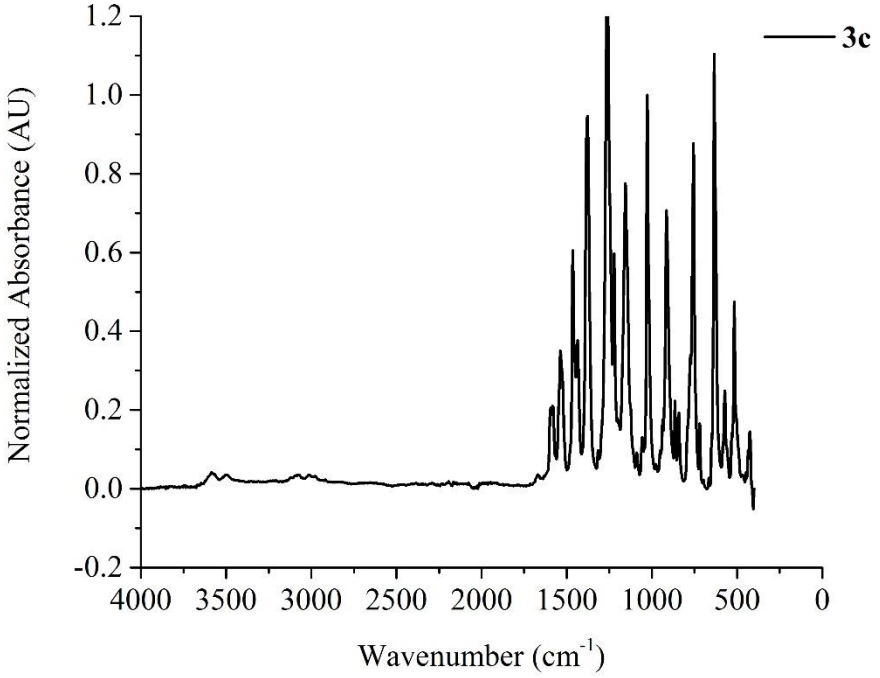

Figure S20. Solid State ATR-FTIR spectrum of [(TMTAA]V═O→Co(Py_5Me_2)](CF_3SO_3)$_2$ (**3c**).

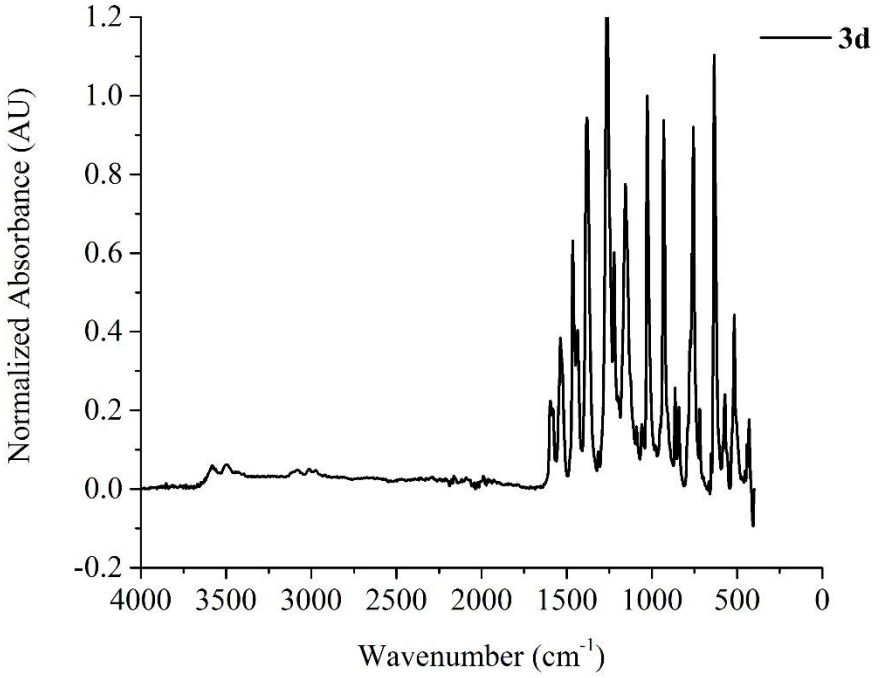

Figure S21. Solid State ATR-FTIR spectrum of [(TMTAA]V═O→Ni(Py_5Me_2)](CF_3SO_3)$_2$ (**3d**).

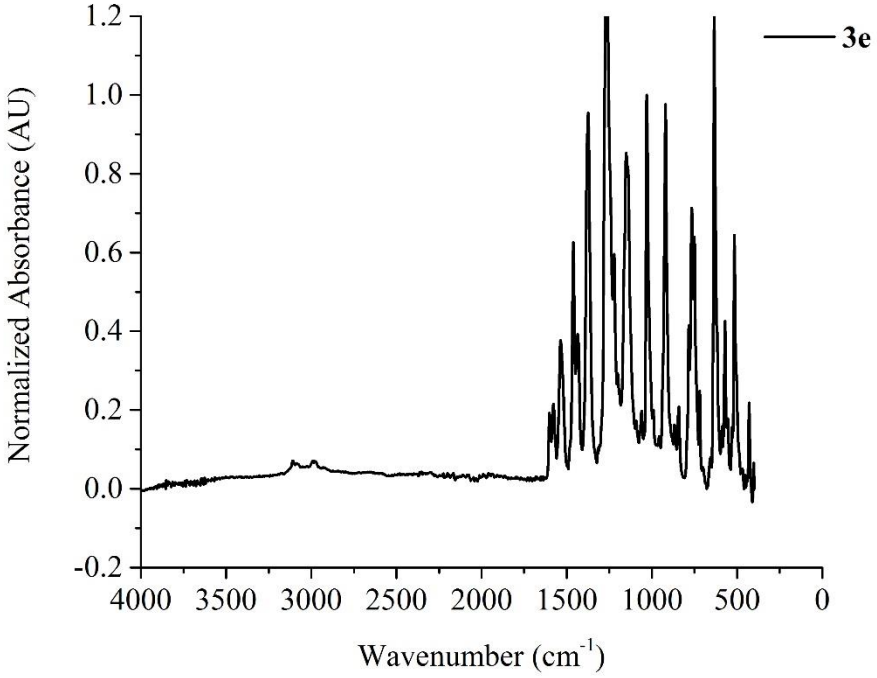

Figure S22. Solid State ATR-FTIR spectrum of [(TMTAA]V═O→Cu(Py_5Me_2)](CF_3SO_3)$_2$ (**3e**).

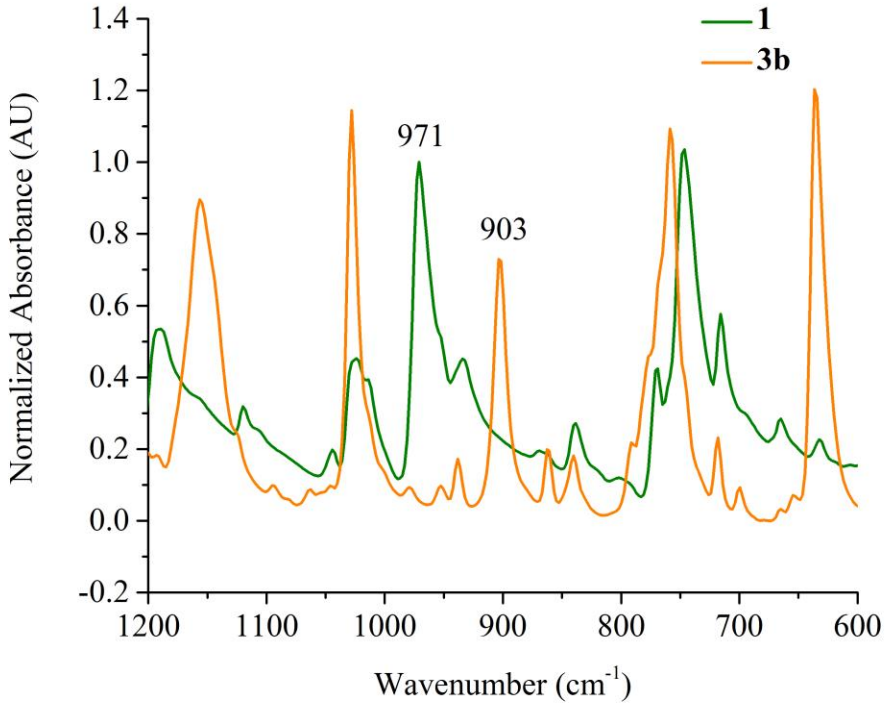

Figure S23. Overlay of ATR-FTIR spectra of **1** and **3b**.

ESI-HRMS Results

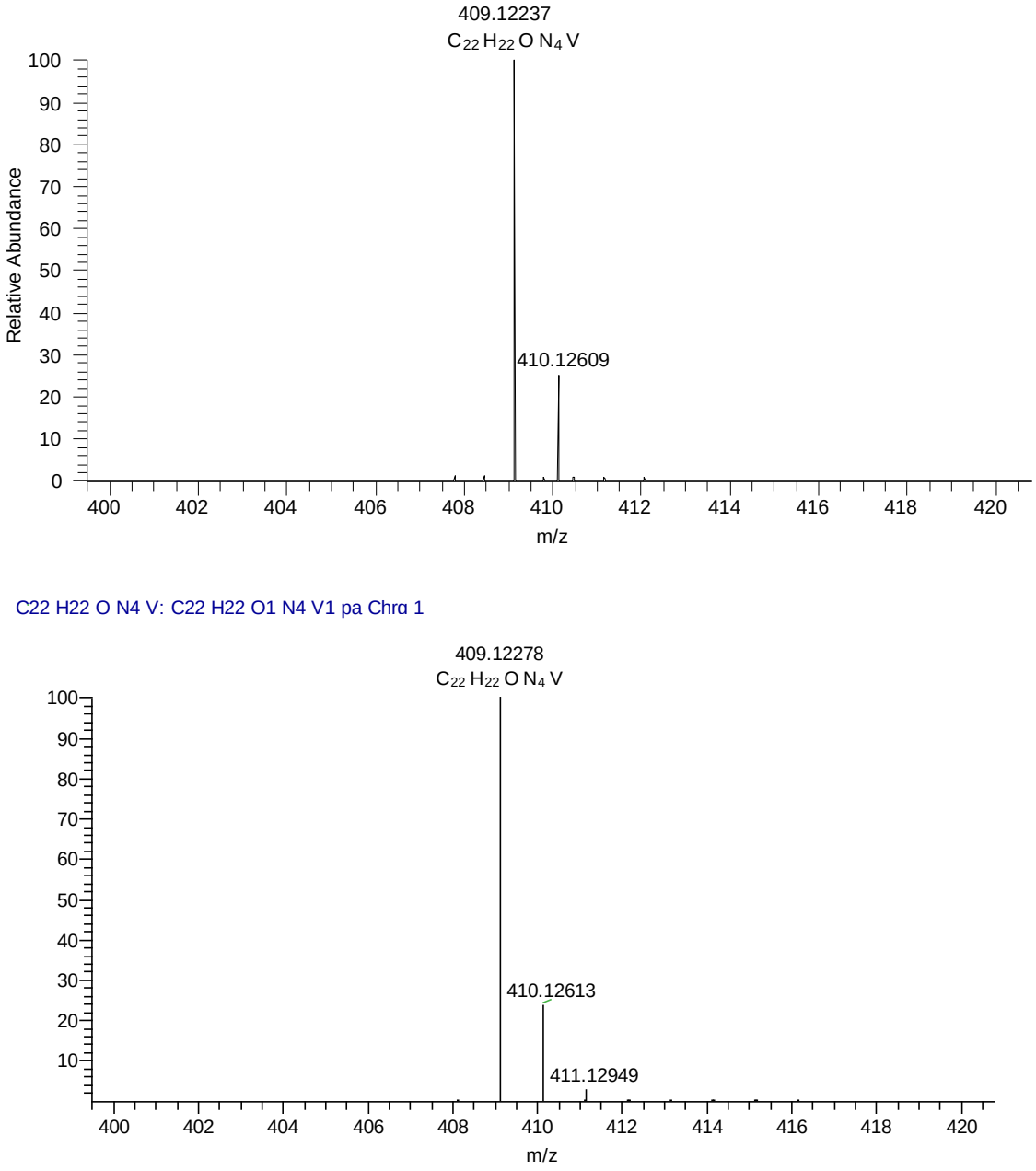

Figure S24. ESI-HRMS result of (TMTAA)V═O (**1**). Above: Experimental result. Below: Simulated spectrum.

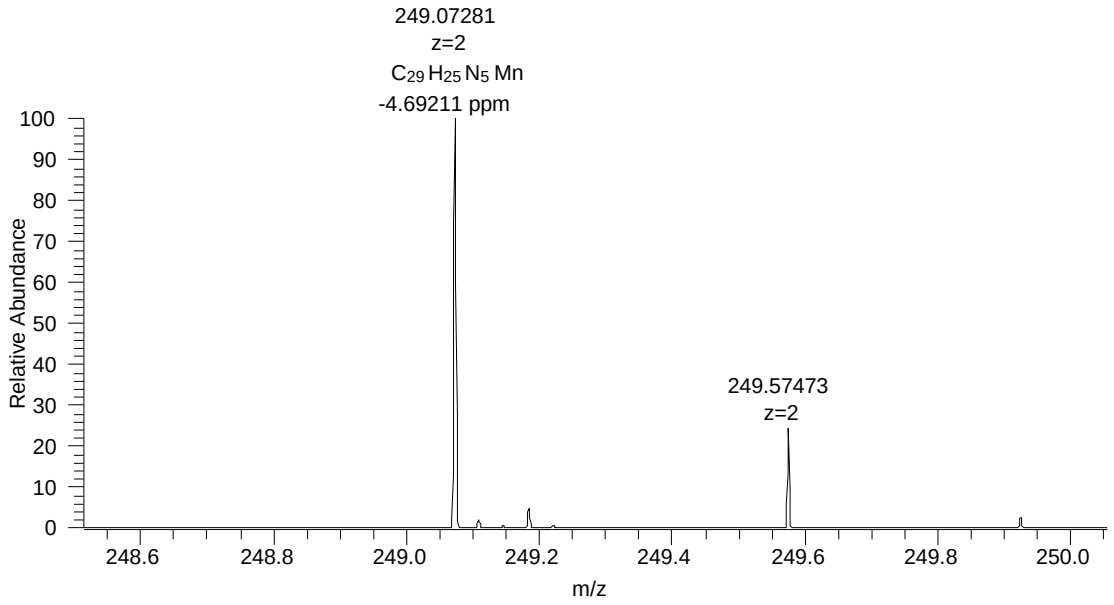

C29 H25 N5 Mn: C29 H25 N5 Mn1 pa Chrg 2

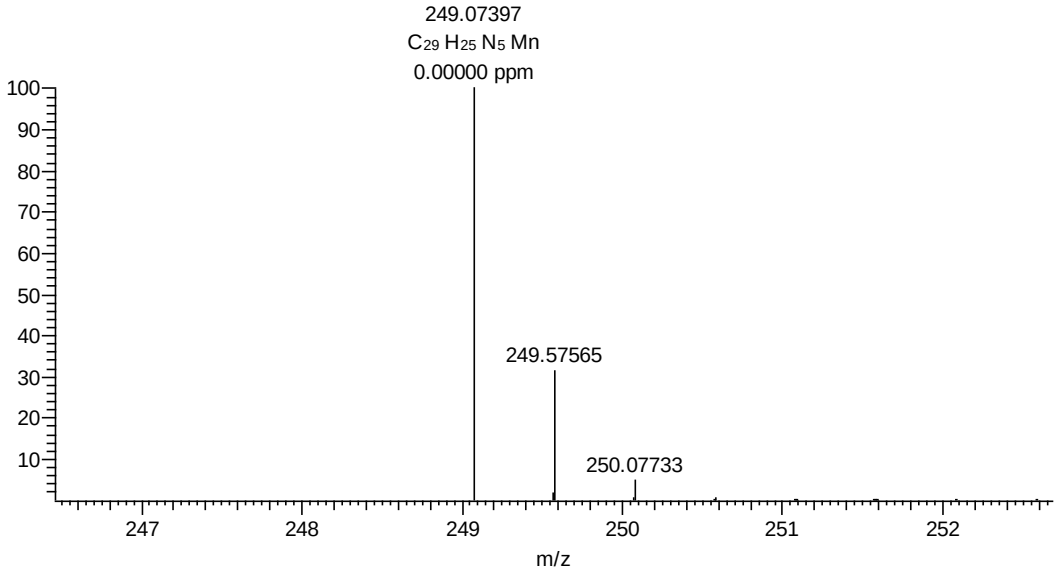

Figure S25. ESI-HRMS result of $[Mn(Py_5Me_2)](CF_3SO_3)_2$ (**2a**). Above: Experimental result. Below: Simulated spectrum.

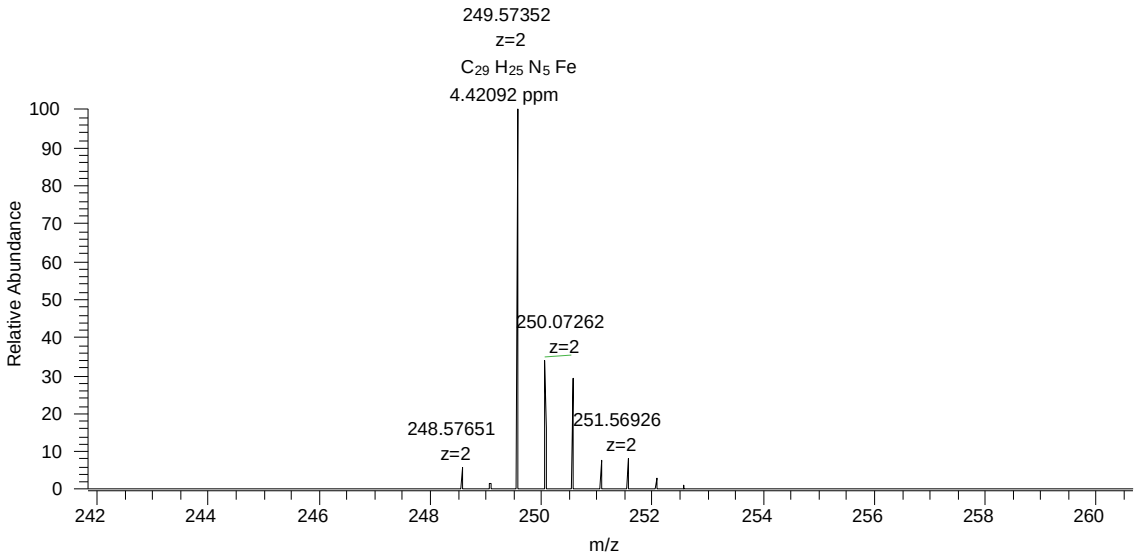

C29 H25 N5 Fe: C29 H25 N5 Fe1 pa Chrg 2

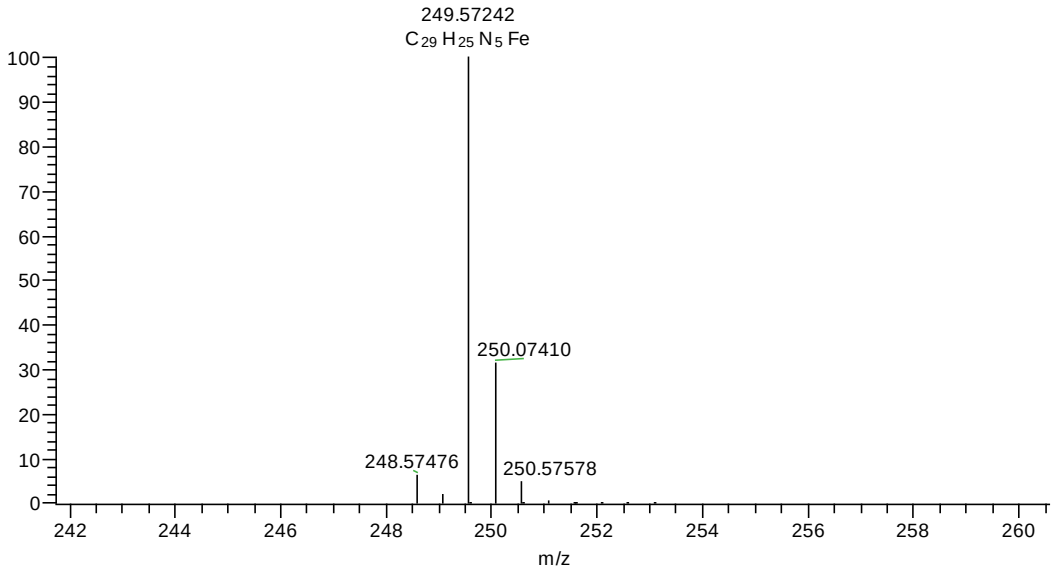

Figure S26. ESI-HRMS result of [Fe(Py_5Me_2)](CF_3SO_3)$_2$ (**2b**). Above: Experimental result. Below: Simulated spectrum.

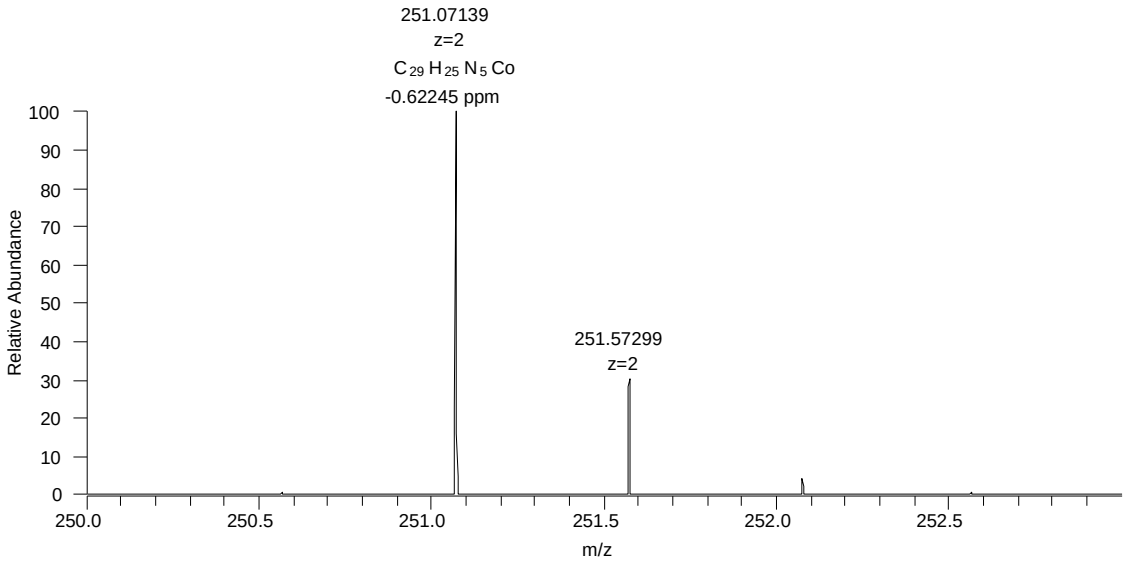

C29 H25 N5 Co: C29 H25 N5 Co1 pa Chrg 2

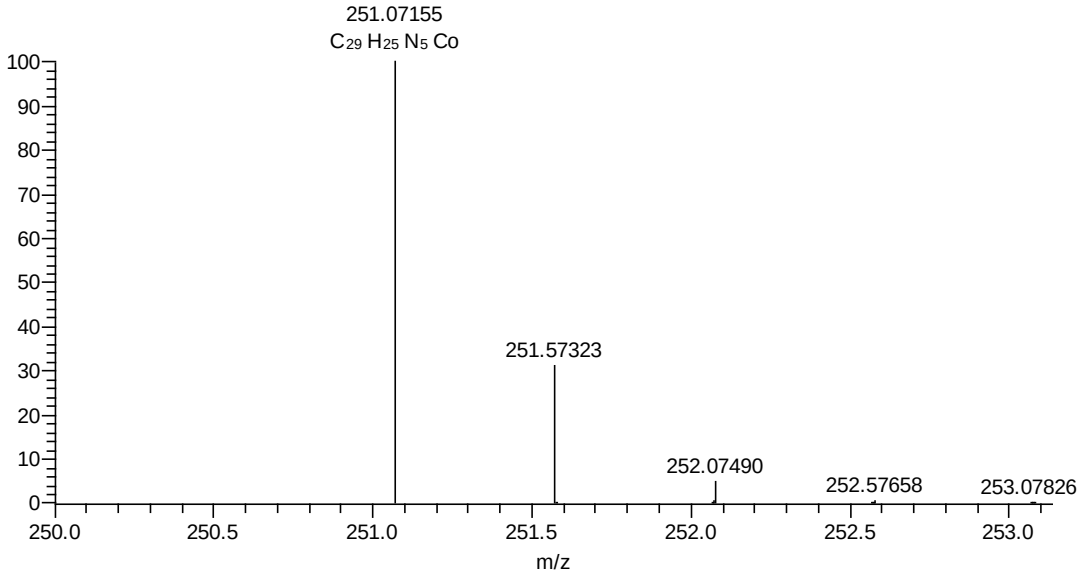

Figure S27. ESI-HRMS result of [Co(Py_5Me_2)](CF_3SO_3)$_2$ (**2c**). Above: Experimental result. Below: Simulated spectrum.

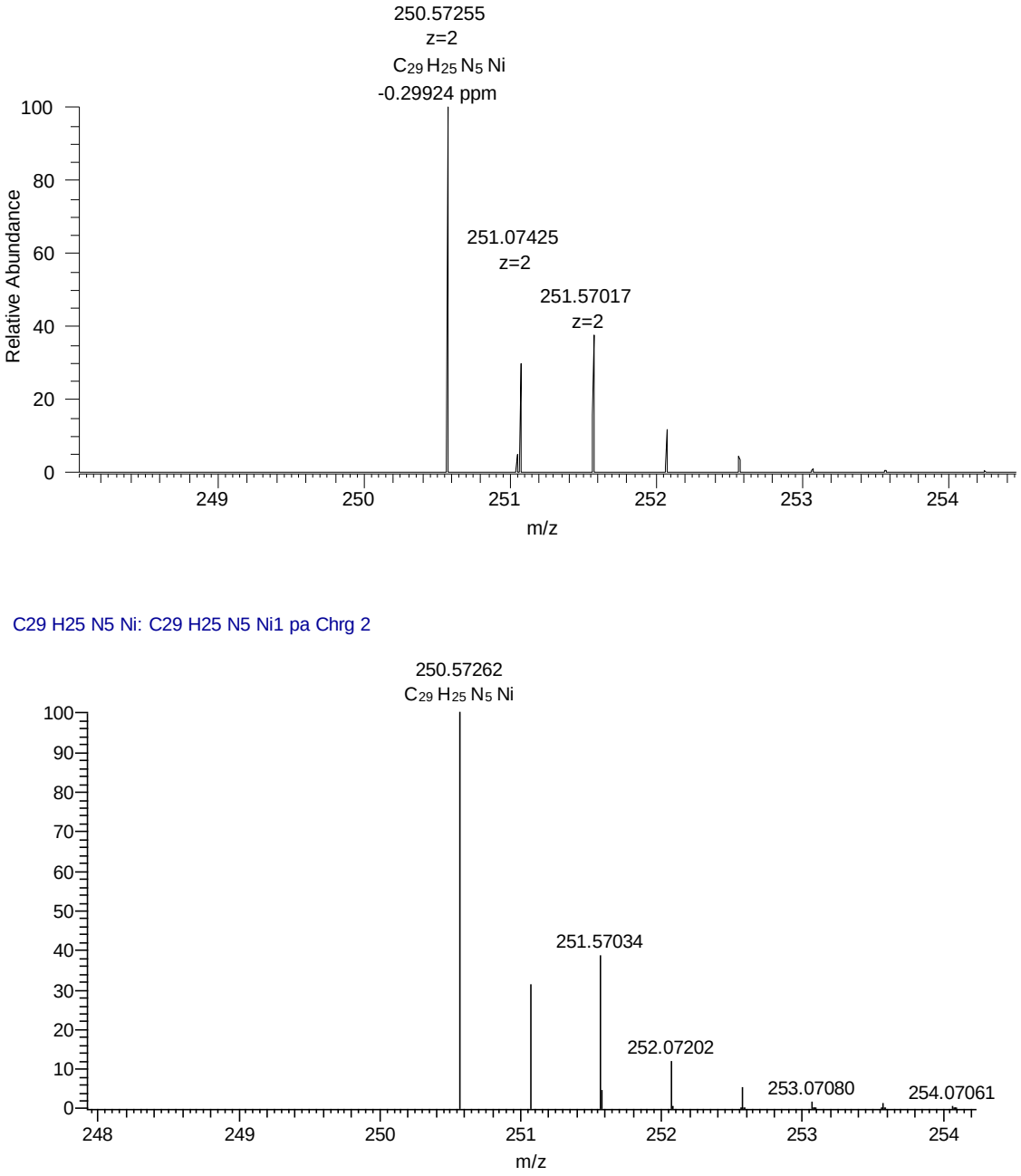

Figure S28. ESI-HRMS result of $[Ni(Py_5Me_2)](CF_3SO_3)_2$ (**2d**). Above: Experimental result. Below: Simulated spectrum.

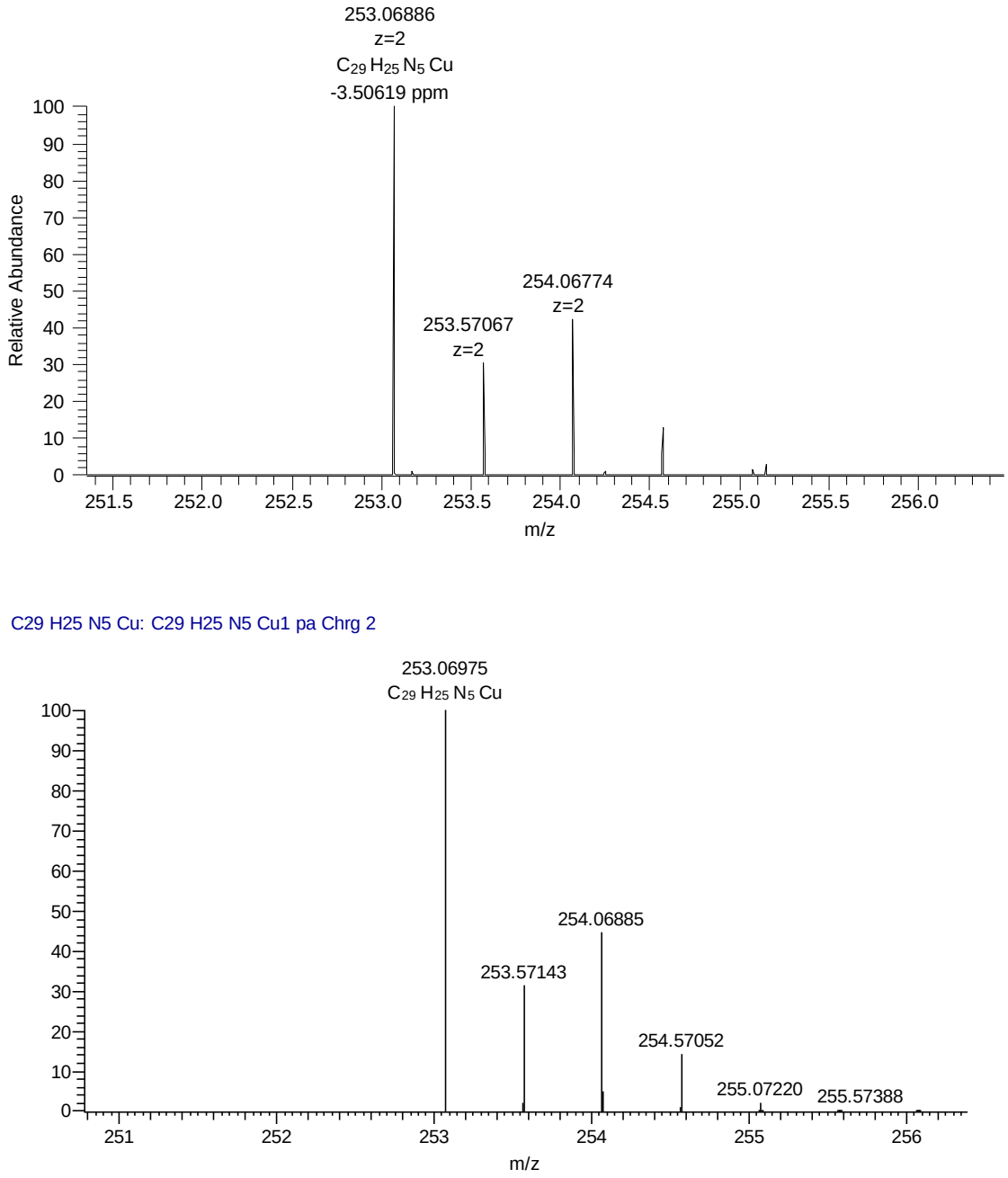

Figure S29. ESI-HRMS result of $[Cu(Py_5Me_2)](CF_3SO_3)_2$ (**2e**). Above: Experimental result. Below: Simulated spectrum.

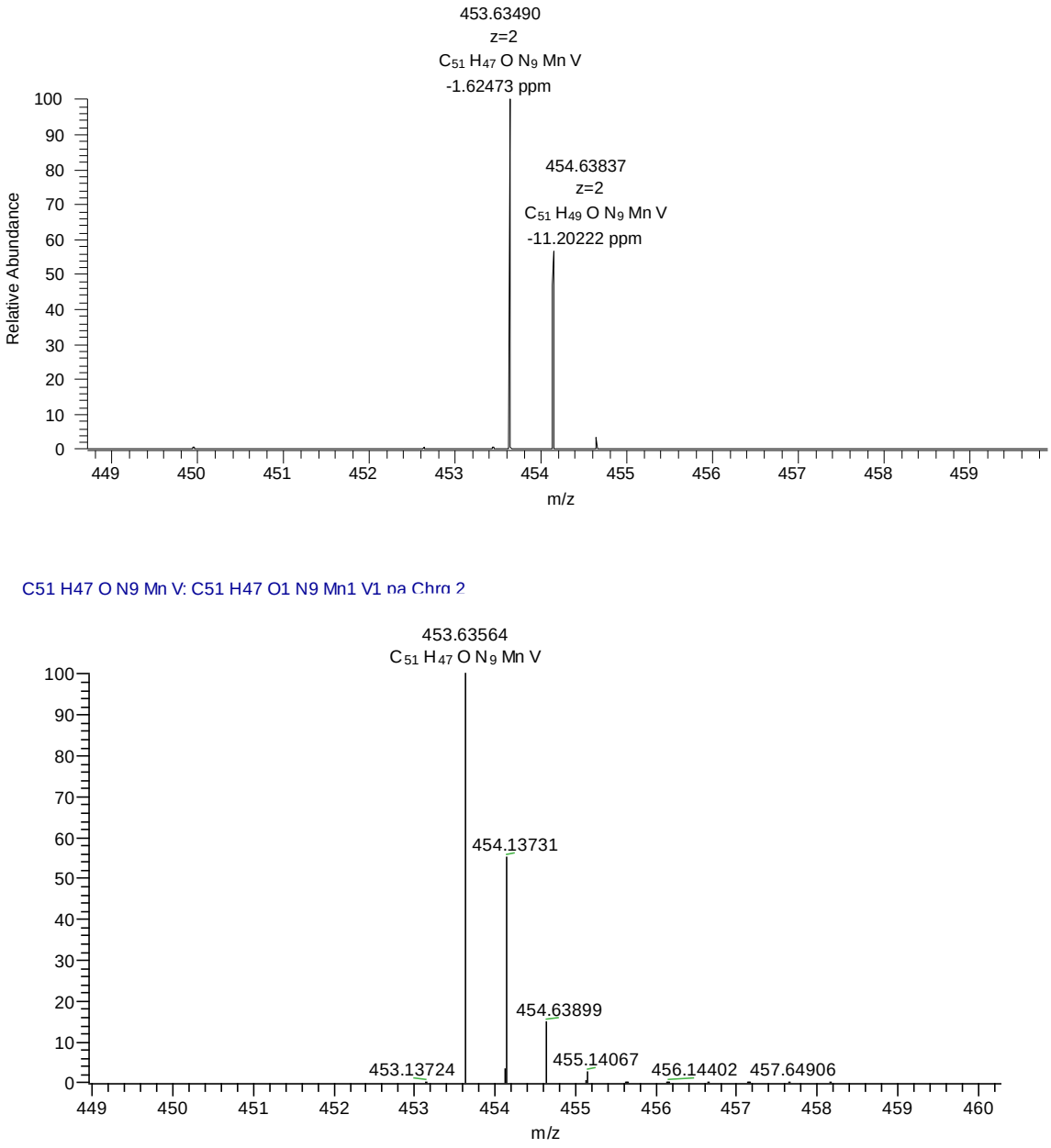

Figure S30. ESI-HRMS result of [(TMTAA]V═O→Mn(Py_5Me_2)](CF_3SO_3)$_2$ (**3a**). Above: Experimental result. Below: Simulated spectrum.

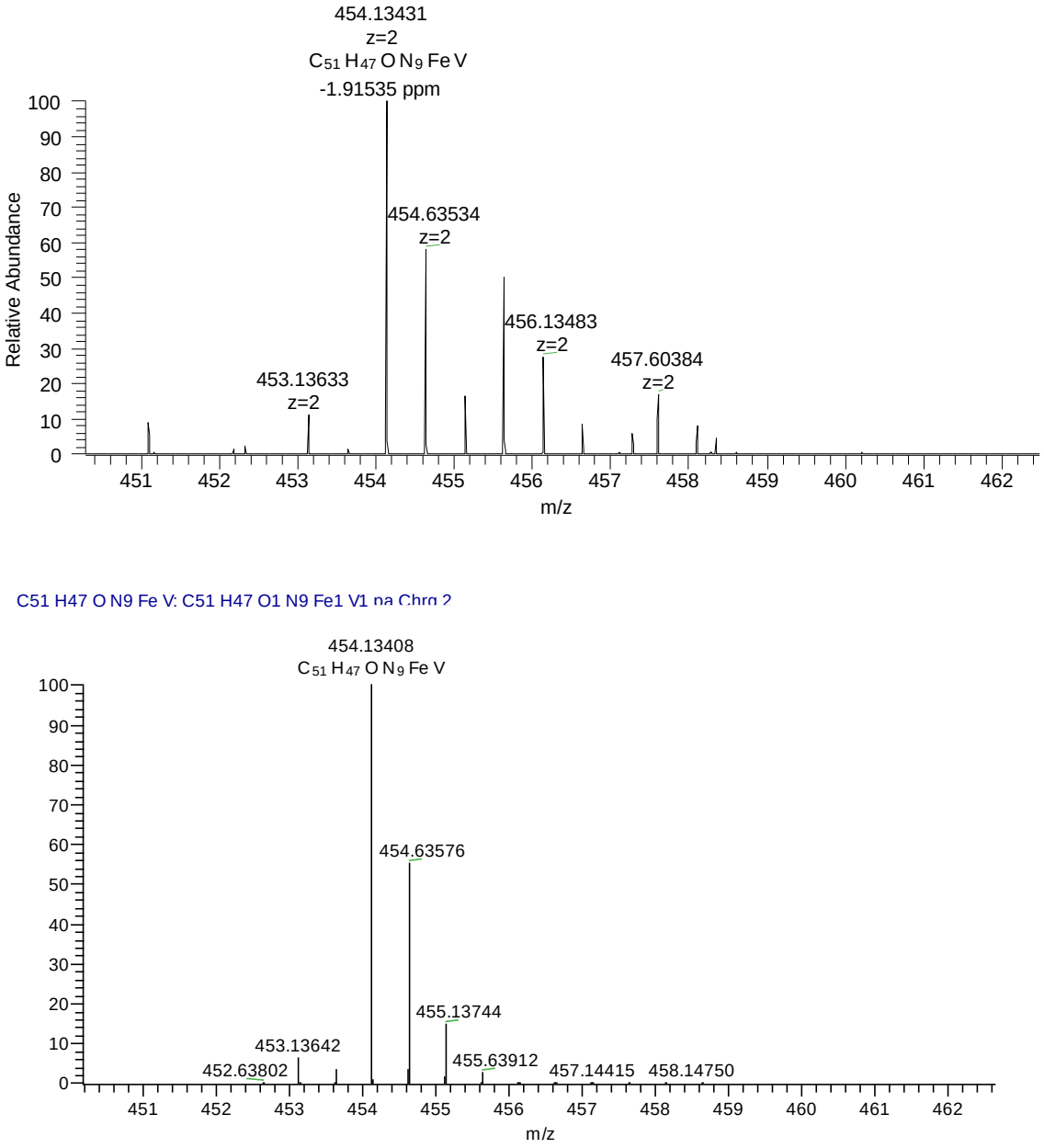

Figure S31. ESI-HRMS result of [(TMTAA]V═O→Fe(Py_5Me_2)](CF_3SO_3)$_2$ (**3b**). Above: Experimental result. Below: Simulated spectrum.

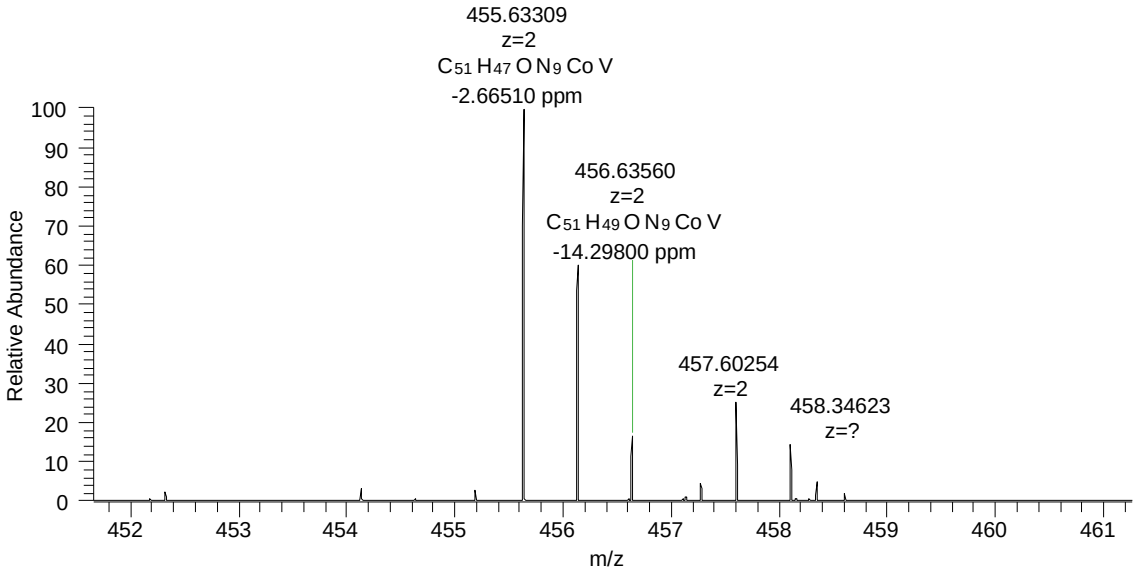

C51 H47 O N9 Co V: C51 H47 O1 N9 Co1 V1 pa Chrg 2

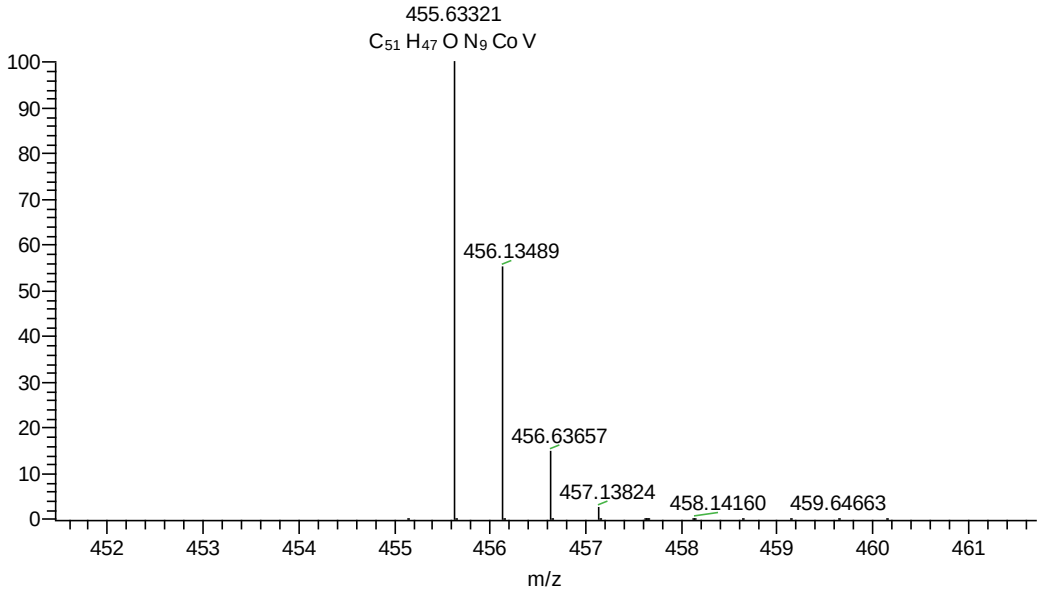

Figure S32. ESI-HRMS result of [(TMTAA]V═O→Co(Py_5Me_2)](${CF_3SO_3}_2$ (**3c**). Above: Experimental result. Below: Simulated spectrum.

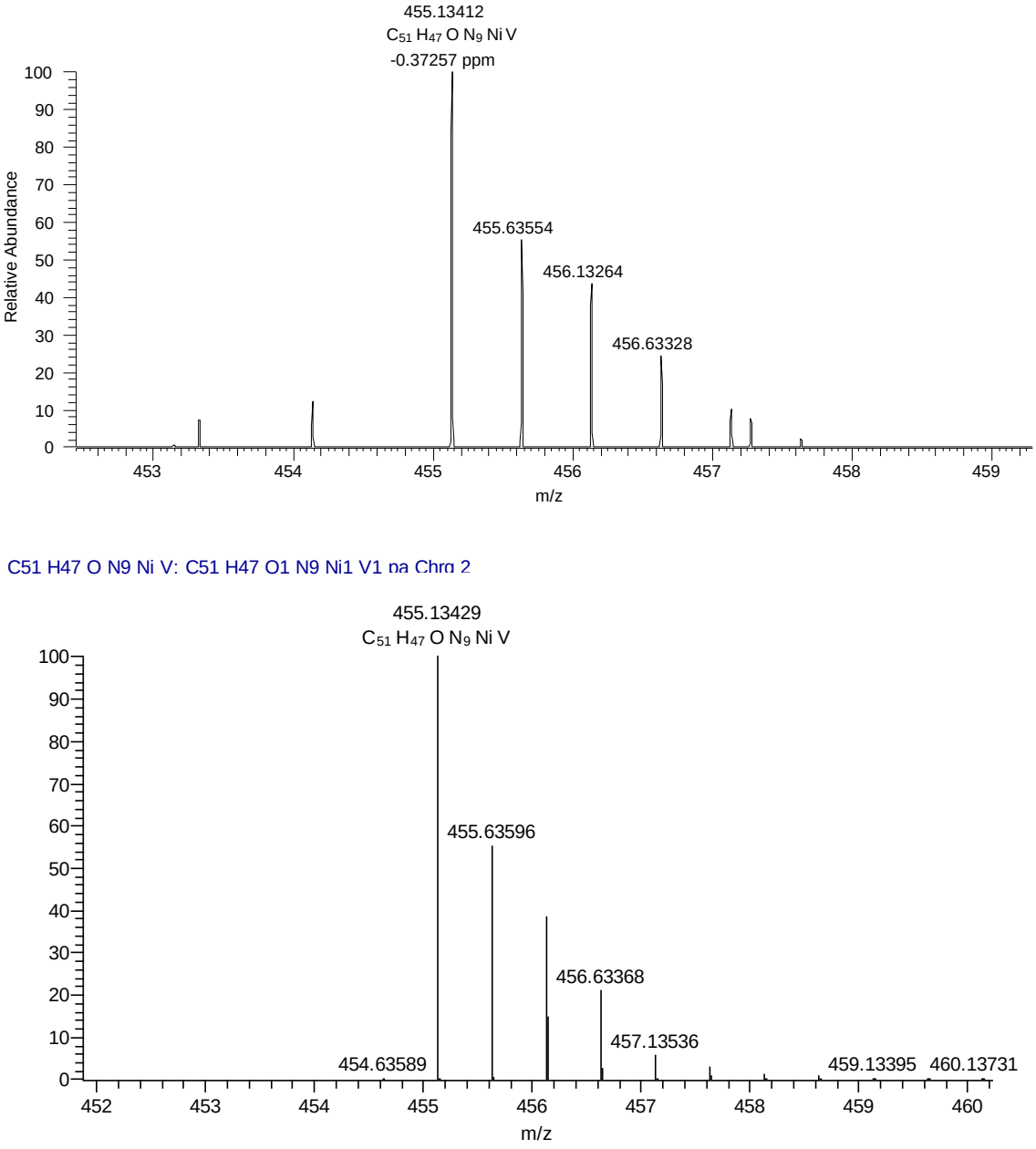

Figure S33. ESI-HRMS result of [(TMTAA]V═O→Ni(Py_5Me_2)](CF_3SO_3)$_2$ (**3d**). Above: Experimental result. Below: Simulated spectrum.

Crystallographic Details

Table S1. Crystal data and structure refinement of **3a**.

Empirical formula	$C_{56}H_{53}F_6MnN_9O_8S_2V$
Formula weight	1264.07
Temperature (K)	110(2)
Wavelength (Å)	0.71073
Crystal System	triclinic
Space Group	$P\bar{1}$
a (Å)	13.2168(3)
b (Å)	13.4371(3)
c (Å)	18.6579(4)
α (°)	102.5680(10)
β (°)	96.7380(10)
γ (°)	118.6840(10)
Volume (Å^3)	2740.45(11)
Z	2
ρ_{calcd} (g/cm^3)	1.532
Absorption coefficient (mm^{-1})	0.562
F(000)	1300
Crystal Size (mm^3)	0.220 × 0.310 × 0.330
θ range for data collection (°)	1.82 to 31.59
Reflections collected	101147
Independent reflections	18356 [R_{int} = 0.0281]
Data/restraints/parameters	18356 / 57 / 789
Goodness-of-fit on F^2	1.027
Refinement Method	Full-matrix least-squares on F^2
Final R indices [I>2σ(I)]	R_1 = 0.0498, wR_2 = 0.1310
R indices (all data)	R_1 = 0.0605, wR_2 = 0.1394
Largest diff. peak/hole (e. Å^3)	1.850/-1.194

All crystal structure determinations were performed with a Bruker-Nonius X8 Kappa Apex2 diffractometer using MoKα radiation at a temperature of 110K. Suitable crystals of were selected under the microscope and mounted on MiTeGen mount using a minimum amount of Paratone N oil. Data were corrected for absorption and polarization effects using multi-scan methods (SADABS). The SQUEEZE procedure was implemented in PLATON in order to subtract out the solvent's contribution to the diffraction pattern. Structures were solved using direct methods. H atoms were placed at calculated positions and their isotropic displacement parameters refined as "riding" on the non-H atom to which they are bonded. Graphic representations of the resulting structure were produced using OLEX 2.

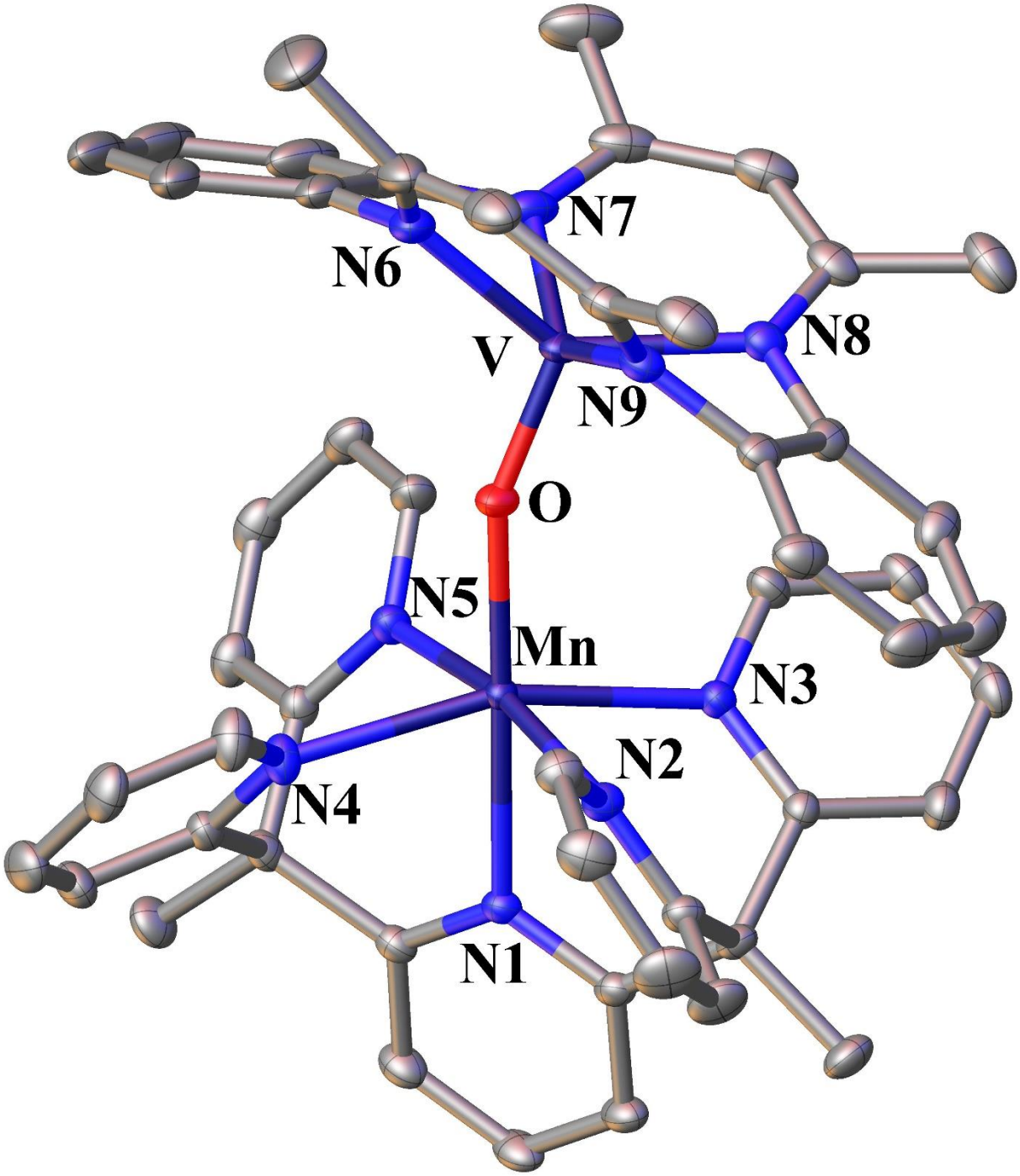

Figure S34. X-ray crystal structure of $[(TMTAA]V{=}O{\rightarrow}Mn(Py_5Me_2)]^{2+}$ (**3a**) with thermal ellipsoids drawn at the 50% probability level.

Table S2. Crystal data and structure refinement of **3b**.

Empirical formula	$C_{53}H_{49}F_6FeN_9O_8S_2V$
Formula weight	1224.92
Temperature (K)	110(2)
Wavelength (Å)	0.71073
Crystal System	monoclinic
Space Group	$P2_1/n$
a (Å)	18.2672(11)
b (Å)	15.7643(10)
c (Å)	18.8744(11)
α (°)	90
β (°)	113.486(2)
γ (°)	90
Volume (Å^3)	5012.3(5)
Z	4
ρ_{calcd} (g/cm^3)	1.623
Absorption coefficient (mm^{-1})	0.650
F(000)	2516
Crystal Size (mm^3)	0.036 × 0.338 × 0.407
θ range for data collection (°)	1.31 to 23.82
Reflections collected	58071
Independent reflections	7711 [R_{int} = 0.0499]
Data/restraints/parameters	7711 / 0 / 730
Goodness-of-fit on F^2	1.030
Refinement Method	Full-matrix least-squares on F^2
Final R indices [I>2σ(I)]	R_1 = 0.0356, wR_2 = 0.0844
R indices (all data)	R_1 = 0.0520, wR_2 = 0.0933
Largest diff. peak/hole (e. Å^3)	0.782/-0.529

All crystal structure determinations were performed with a Bruker-Nonius X8 Kappa Apex2 diffractometer using MoKα radiation at a temperature of 110K. Suitable crystals of were selected under the microscope and mounted on MiTeGen mount using a minimum amount of Paratone N oil. Data were corrected for absorption and polarization effects using multi-scan methods (SADABS). The SQUEEZE procedure was implemented in PLATON in order to subtract out the solvent's contribution to the diffraction pattern. Structures were solved using direct methods. H atoms were placed at calculated positions and their isotropic displacement parameters refined as "riding" on the non-H atom to which they are bonded. Graphic representations of the resulting structure were produced using OLEX 2.

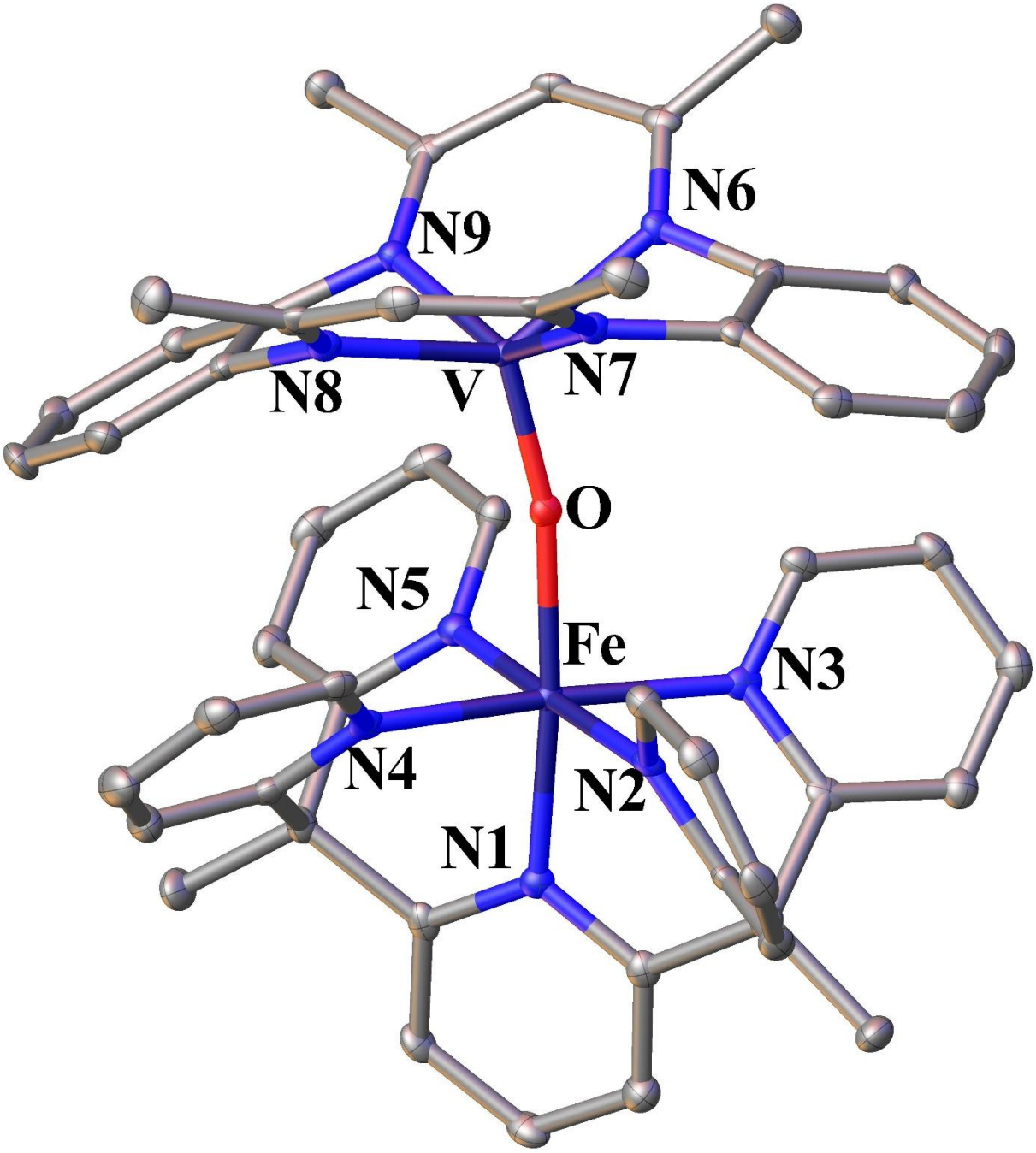

Figure S35. X-ray crystal structure of $[(TMTAA]V{=}O{\rightarrow}Fe(Py_5Me_2)]^{2+}$ (**3b**) with thermal ellipsoids drawn at the 50% probability level.

Table S3. Crystal data and structure refinement of **3c**.

Empirical formula	$C_{53}H_{49}CoF_6N_9O_8S_2V$
Formula weight	1228.00
Temperature (K)	110(2)
Wavelength (Å)	0.71073
Crystal System	monoclinic
Space Group	$P2_1/n$
a (Å)	18.3347(11)
b (Å)	15.7616(10)
c (Å)	19.1765(12)
α (°)	90
β (°)	113.480(2)
γ (°)	90
Volume ($Å^3$)	5082.8(5)
Z	4
ρ_{calcd} (g/cm^3)	1.605
Absorption coefficient (mm^{-1})	0.681
F(000)	2520
Crystal Size (mm^3)	0.052 × 0.207 × 0.486
θ range for data collection (°)	1.30 to 25.36
Reflections collected	61702
Independent reflections	9302 [R_{int} = 0.0567]
Data/restraints/parameters	9302 / 0 / 730
Goodness-of-fit on F^2	1.040
Refinement Method	Full-matrix least-squares on F^2
Final R indices [I>2σ(I)]	R_1 = 0.0373, wR_2 = 0.0840
R indices (all data)	R_1 = 0.0609, wR_2 = 0.0943
Largest diff. peak/hole (e. $Å^3$)	0.628/-0.459

All crystal structure determinations were performed with a Bruker-Nonius X8 Kappa Apex2 diffractometer using MoKα radiation at a temperature of 110K. Suitable crystals of were selected under the microscope and mounted on MiTeGen mount using a minimum amount of Paratone N oil. Data were corrected for absorption and polarization effects using multi-scan methods (SADABS). The SQUEEZE procedure was implemented in PLATON in order to subtract out the solvent's contribution to the diffraction pattern. Structures were solved using direct methods. H atoms were placed at calculated positions and their isotropic displacement parameters refined as "riding" on the non-H atom to which they are bonded. Graphic representations of the resulting structure were produced using OLEX 2.

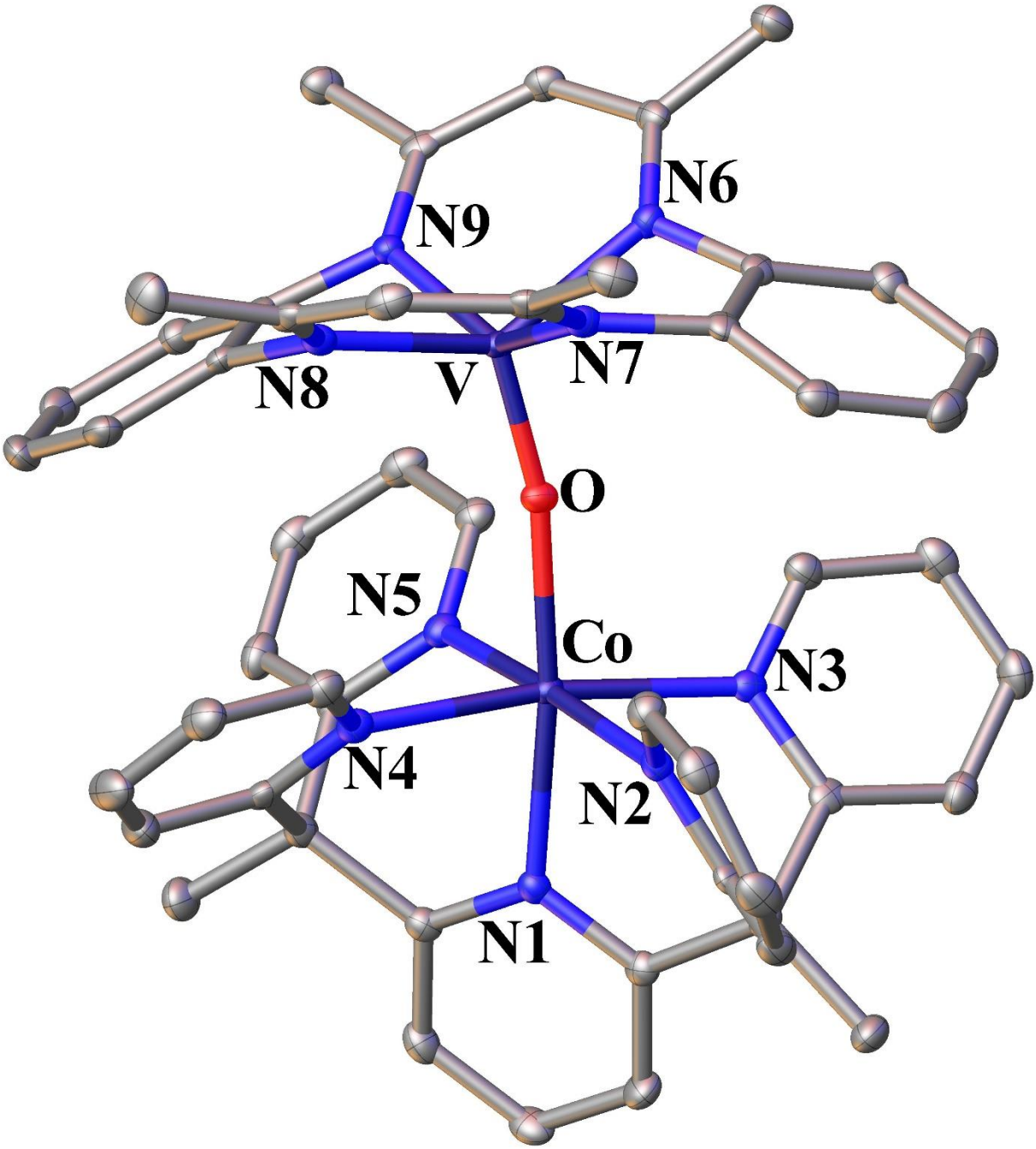

Figure S36. X-ray crystal structure of $[(TMTAA]V{=}O{\rightarrow}Co(Py_5Me_2)]^{2+}$ (**3c**) with thermal ellipsoids drawn at the 50% probability level.

Table S4. Crystal data and structure refinement of **3d**.

Empirical formula	$C_{53}H_{49}F_6N_9NiO_8S_2V$
Formula weight	1227.78
Temperature (K)	110(2)
Wavelength (Å)	0.71073
Crystal System	monoclinic
Space Group	$P2_1/n$
a (Å)	18.3482(6)
b (Å)	15.7837(4)
c (Å)	19.1046(6)
α (°)	90
β (°)	113.556(2)
γ (°)	90
Volume ($Å^3$)	5071.7(3)
Z	4
ρ_{calcd} (g/cm^3)	1.608
Absorption coefficient (mm^{-1})	0.727
F(000)	2524
Crystal Size (mm^3)	0.050 × 0.260 × 0.272
θ range for data collection (°)	1.30 to 25.68
Reflections collected	60975
Independent reflections	9624 [R_{int} = 0.0487]
Data/restraints/parameters	9624 / 754 / 733
Goodness-of-fit on F^2	1.013
Refinement Method	Full-matrix least-squares on F^2
Final R indices [I>2σ(I)]	R_1 = 0.0336, wR_2 = 0.0744
R indices (all data)	R_1 = 0.0541, wR_2 = 0.0825
Largest diff. peak/hole (e. $Å^3$)	0.673/-0.432

All crystal structure determinations were performed with a Bruker-Nonius X8 Kappa Apex2 diffractometer using MoKα radiation at a temperature of 110K. Suitable crystals of were selected under the microscope and mounted on MiTeGen mount using a minimum amount of Paratone N oil. Data were corrected for absorption and polarization effects using multi-scan methods (SADABS). The SQUEEZE procedure was implemented in PLATON in order to subtract out the solvent's contribution to the diffraction pattern. Structures were solved using direct methods. H atoms were placed at calculated positions and their isotropic displacement parameters refined as "riding" on the non-H atom to which they are bonded. Graphic representations of the resulting structure were produced using OLEX 2.

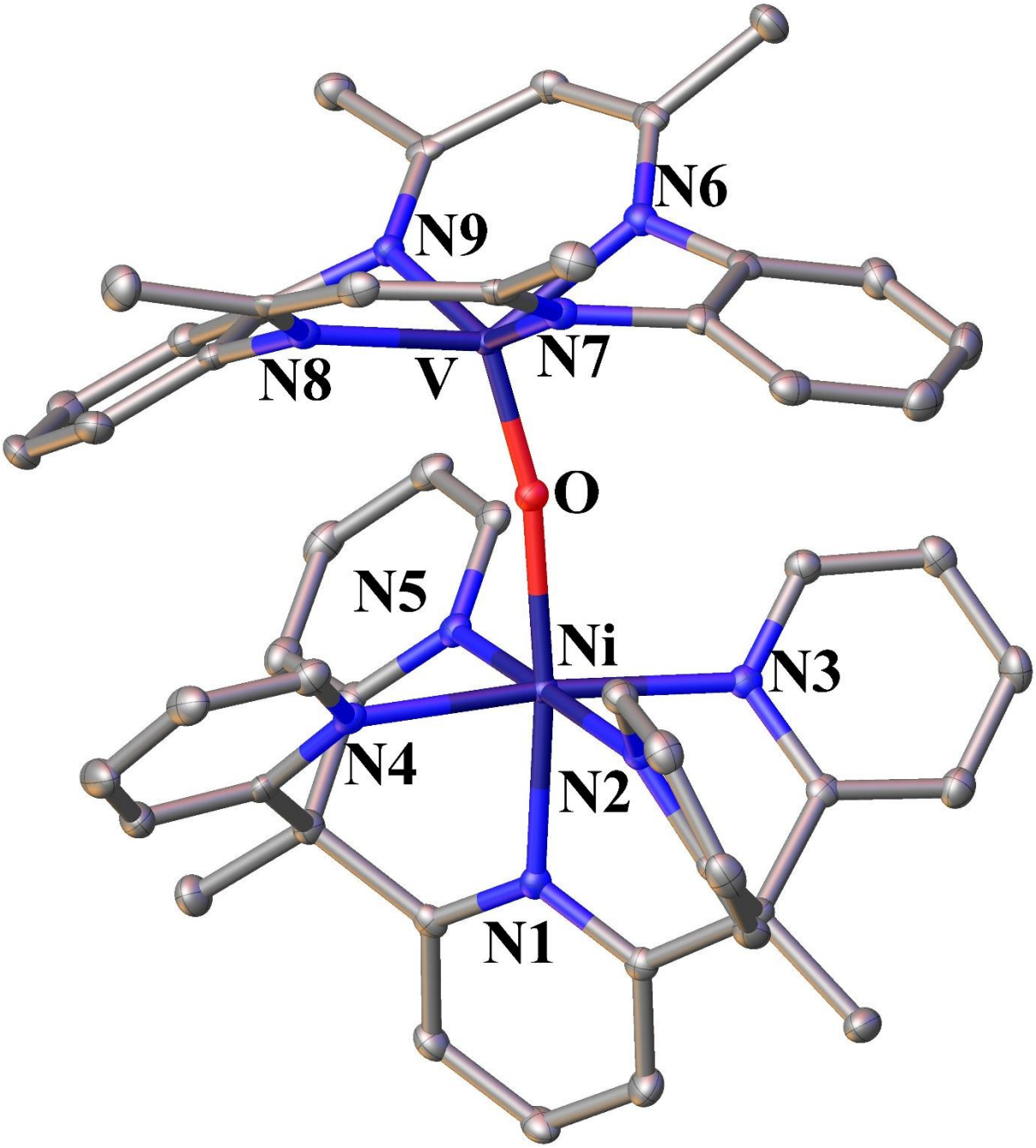

Figure S37. X-ray crystal structure of $[(TMTAA]V{=}O{\rightarrow}Ni(Py_5Me_2)]^{2+}$ (**3d**) with thermal ellipsoids drawn at the 50% probability level.

Table S5. Crystal data and structure refinement of **3e**.

Empirical formula	$C_{53}H_{47}F_6N_9CuO_7S_2V$
Formula weight	1214.59
Temperature (K)	110(2)
Wavelength (Å)	0.71073
Crystal System	monoclinic
Space Group	$P2_1/n$
a (Å)	18.0595(7)
b (Å)	15.3356(6)
c (Å)	20.4359(8)
α (°)	90
β (°)	113.311(2)
γ (°)	90
Volume ($Å^3$)	5197.8(4)
Z	4
ρ_{calcd} (g/cm^3)	1.552
Absorption coefficient (mm^{-1})	0.754
F(000)	2488
Crystal Size (mm^3)	0.200 × 0.220 × 0.240
θ range for data collection (°)	1.28 to 31.51
Reflections collected	90561
Independent reflections	17326 [R_{int} = 0.0314]
Data/restraints/parameters	17326 / 0 / 718
Goodness-of-fit on F^2	1.032
Refinement Method	Full-matrix least-squares on F^2
Final R indices [I>2σ(I)]	R_1 = 0.0411, wR_2 = 0.1113
R indices (all data)	R_1 = 0.0553, wR_2 = 0.1204
Largest diff. peak/hole (e. $Å^3$)	2.579/-1.115

All crystal structure determinations were performed with a Bruker-Nonius X8 Kappa Apex2 diffractometer using MoKα radiation at a temperature of 110K. Suitable crystals of were selected under the microscope and mounted on MiTeGen mount using a minimum amount of Paratone N oil. Data were corrected for absorption and polarization effects using multi-scan methods (SADABS). The SQUEEZE procedure was implemented in PLATON in order to subtract out the solvent's contribution to the diffraction pattern. Structures were solved using direct methods. H atoms were placed at calculated positions and their isotropic displacement parameters refined as "riding" on the non-H atom to which they are bonded. Graphic representations of the resulting structure were produced using OLEX 2.

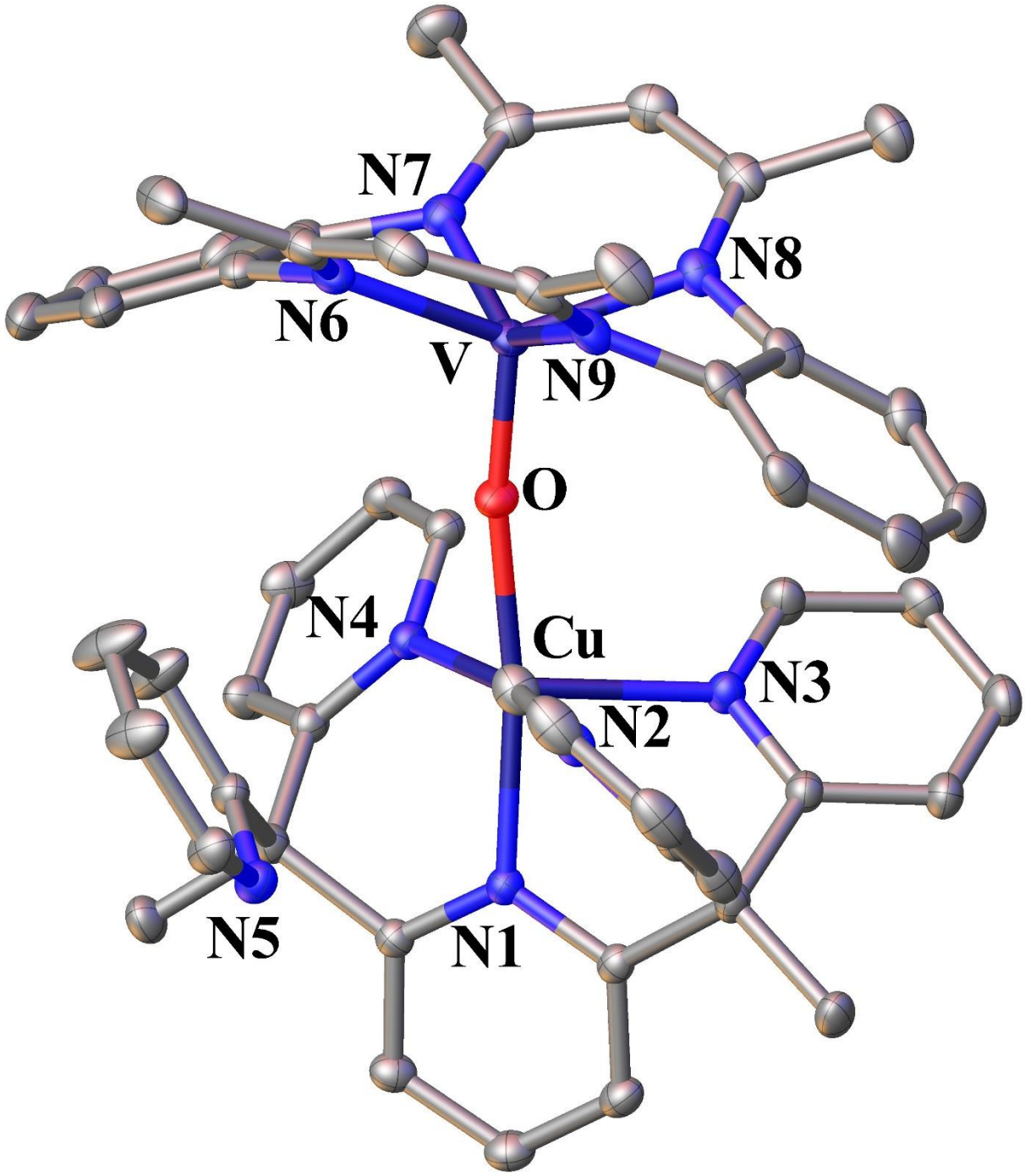

Figure S38. X-ray crystal structure of $[(TMTAA]V{=}O{\rightarrow}Cu(Py_5Me_2)]^{2+}$ (**3e**) with thermal ellipsoids drawn at the 50% probability level.

Electrochemical Experiments

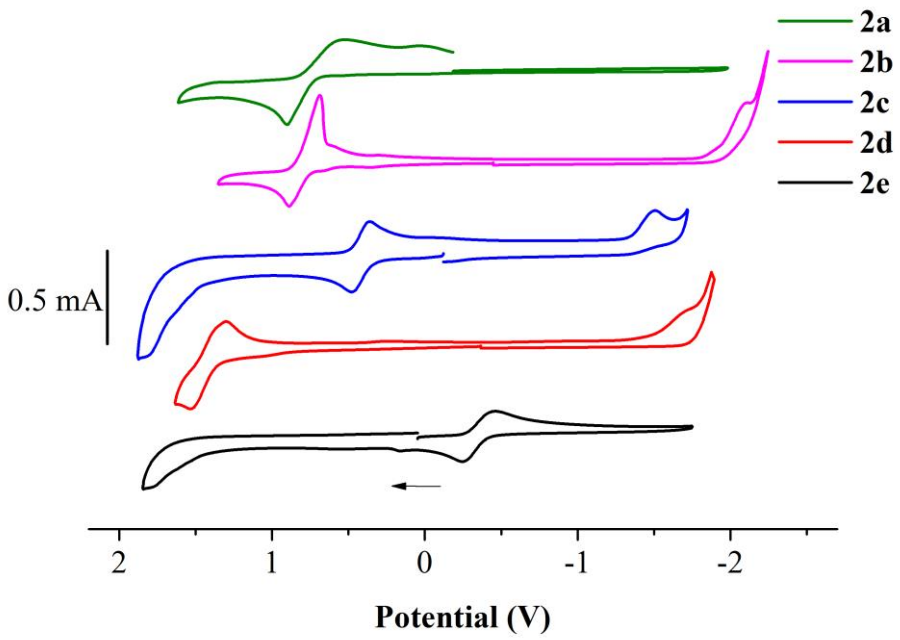

Figure S39. Cyclic voltammograms of **2a-e** in dry dichloromethane under the protection of nitrogen. All signals are referenced to Fc/Fc^{+} (0 V).

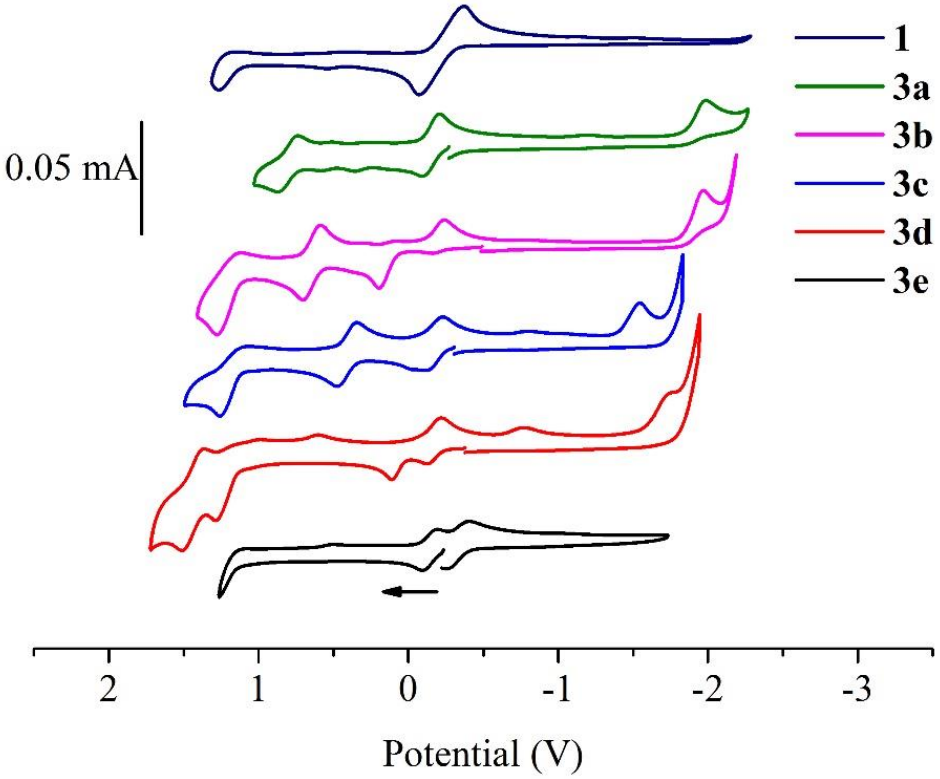

Figure S40. Cyclic voltammograms of **3a-e** in dry dichloromethane under the protection of nitrogen. All signals are referenced to Fc/Fc^{+} (0 V).

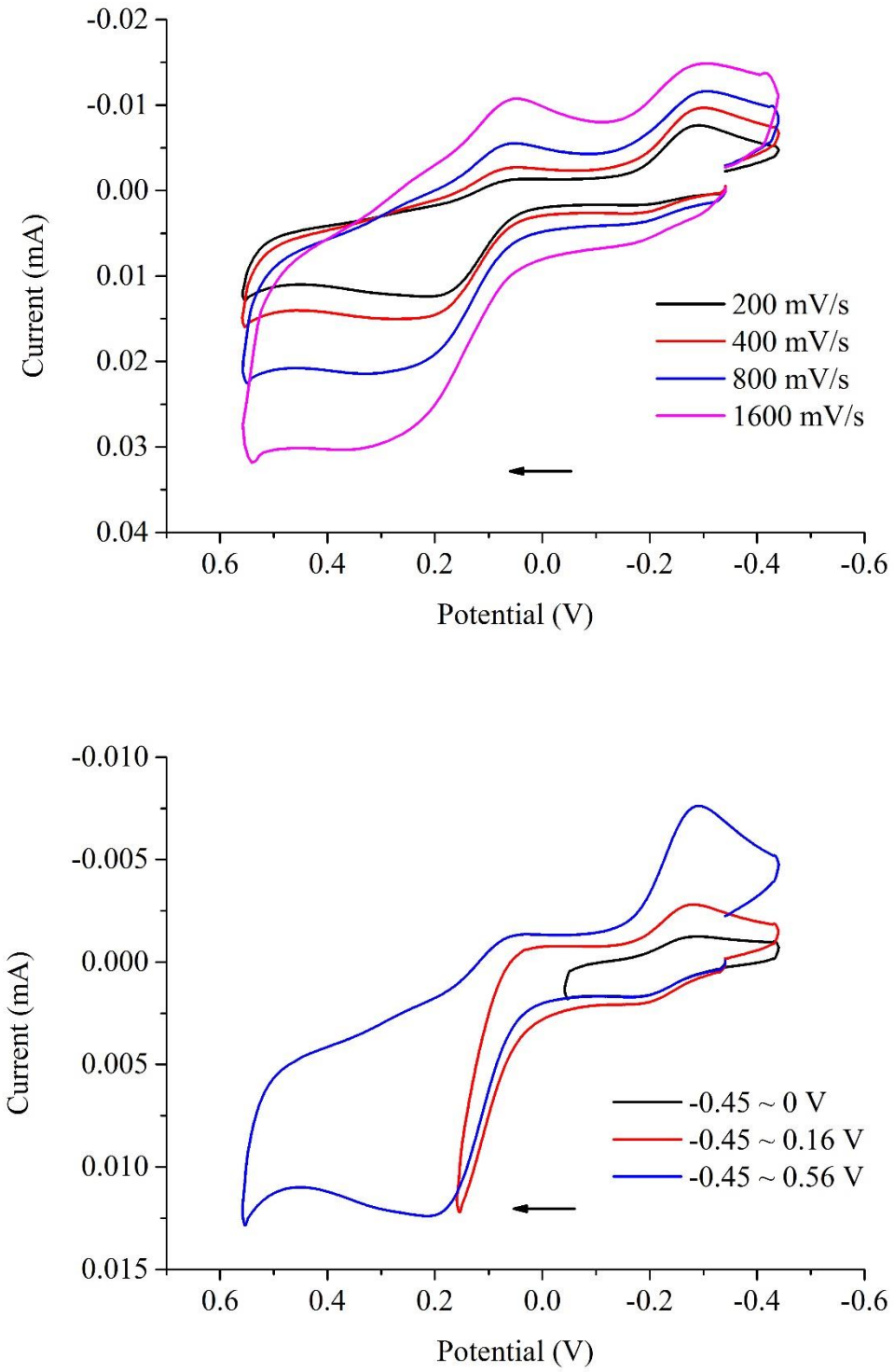

Figure S41. Scan rate study (above) and variable potential scan study (below) on [(TMTAA]V═O→Fe(Py_5Me_2)](CF_3SO_3)$_2$ (**3b**).

Resonance Raman Measurements

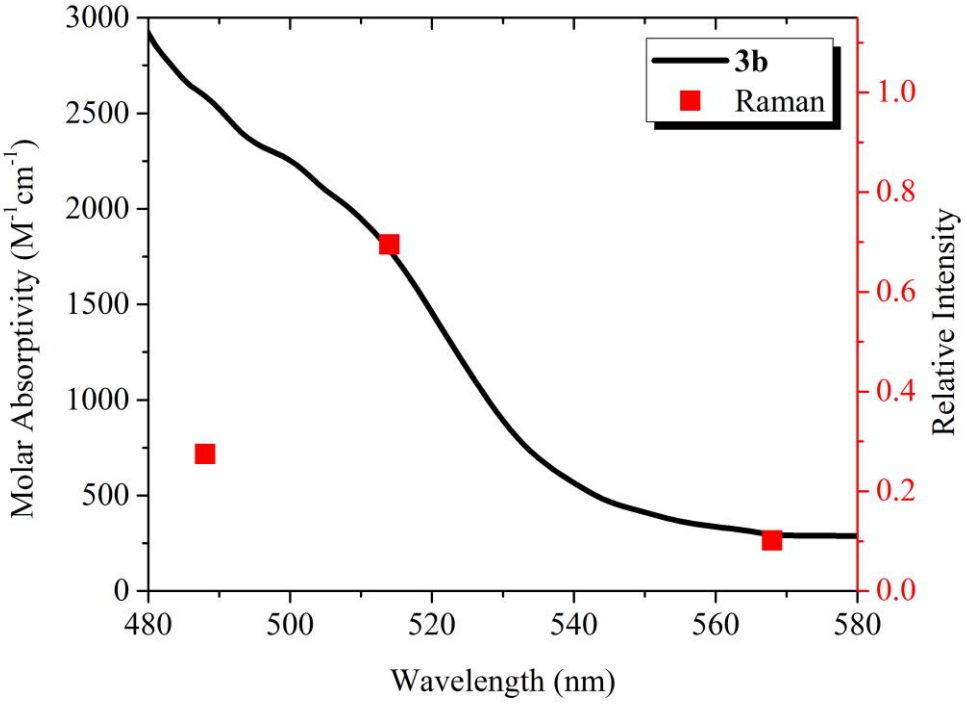

Figure S42. Resonance Raman enhancement profile (dot) overlayed with the EAS spectrum of **3b** (solid curve).

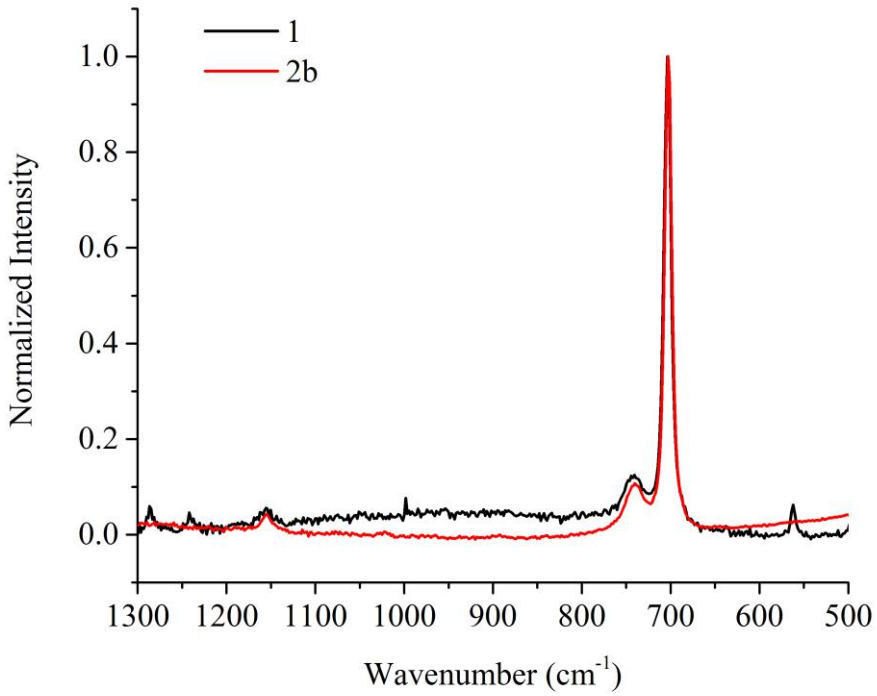

Figure S43. Resonance Raman spectra of **1** and **2b** in dichloromethane. Wavelength and intensity was referenced and normalized to the rRaman signal of dichloromethane at 703 cm^{-1}. Note the absence of any resonance enhanced peak at ~ 900 cm^{-1}.